AGU100 ADVANCING EARTH AND SPACE SCIENCE

Water Resources Research

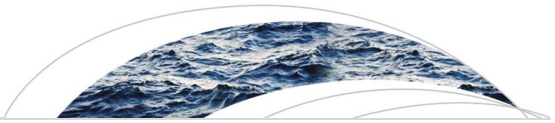

RESEARCH ARTICLE
10.1029/2018WR023165

Key Points:
- Airborne electromagnetic and ground data from the Netherlands are used to quantify differences between commonly used 1-D inversion algorithms
- Qualitatively, inversions are found to be consistent; however, a quantitative analysis on resulting 3-D groundwater salinity volumes highlights significant differences on mapping outcomes
- Out of a total volume of 2.8 billion m^3, a fresh groundwater volume estimate differed by up to 6.5%, depending on the inversion method used; the primary controlling factor on results was found to be model smoothness

Supporting Information:
- Supporting Information S1

Correspondence to:
J. King,
j.a.king@uu.nl

Citation:
King, J., Oude Essink, G., Karaolis, M., Siemon, B., & Bierkens, M. F. P. (2018). Quantifying geophysical inversion uncertainty using airborne frequency domain electromagnetic data—Applied at the province of Zeeland, the Netherlands. *Water Resources Research*, *54*. https://doi.org/10.1029/2018WR023165

Received 20 APR 2018
Accepted 22 SEP 2018
Accepted article online 8 OCT 2018

Quantifying Geophysical Inversion Uncertainty Using Airborne Frequency Domain Electromagnetic Data—Applied at the Province of Zeeland, the Netherlands

Jude King[1,2], Gualbert Oude Essink[1,2], Marios Karaolis[2], Bernhard Siemon[3], and Marc. F. P. Bierkens[1,2]

[1]Department of Physical Geography, Utrecht University, Utrecht, Netherlands, [2]Unit Subsurface and Groundwater Systems, Deltares, Utrecht, Netherlands, [3]Federal Institute for Geosciences and Natural Resources (BGR), Hanover, Germany

Abstract An accurate understanding of the fresh-saline distribution of groundwater is necessary for effective groundwater management. Airborne electromagnetic (AEM) surveys offer a rapid and cost-effective method with which to map this, offering valuable additional information about the subsurface. To convert AEM data into electric conductivity and ultimately groundwater salinity, an inversion is undertaken. A number of algorithms are available for this purpose; however, these are affected by significant uncertainty, owing to inherent nonunique characteristics of this process. The most commonly used inversion codes in hydrogeophysical studies were quantitatively tested using frequency domain AEM and ground data from the province of Zeeland, the Netherlands. These include UBC1DFM code and quasi-2D laterally constrained inversions. Following an investigation of inversion parameter settings, data were inverted for four inversion methods and interpolated into 3-D volumes. Using geological data and empirical electrical conductivity and water salinity relationships, each inversion was converted into groundwater electrical conductivity and split into fresh-brackish-saline regions. For groundwater volume estimates out of a total volume of 2.8 billion m^3, a fresh groundwater estimate could differ by as much as 178 million m^3, depending on the inversion used. The primary factor here was the choice of model smoothness, which was shown to affect the thickness of the brackish interval. Fresh-brackish-saline interfaces were consistently mapped with an accuracy of ~3 m, the brackish being the most accurately resolved. The few layer method was less successful at resolving smoothly varying salinity distributions but more successful at mapping the brackish interface at greater depth.

Plain Language Summary Understanding the current distribution of groundwater salinity in low-elevation coastal zones is important because globally over 600 million people live and potentially rely on fresh groundwater in these areas. Fresh groundwater is also vulnerable to a process called saline intrusion, where usable groundwater can be displaced by less-usable saline groundwater. Groundwater salinity on more regional scales is currently mapped by an instrument that is towed beneath a helicopter. This technique measures electromagnetic responses that relate mostly to salinity variations within groundwater reserves. For these measurements to make sense, they need to be transformed into units that can physically relate to groundwater salinity. This process is called inversion. However, as this procedure comes with significant uncertainty, there are a number of different algorithms available for this. Here we used airborne and ground data from the province of Zeeland, the Netherlands, and tested eight inversion algorithms that are commonly used for this purpose. Results indicate that based on the inversion type, fresh groundwater estimates in a volume of 2.8 billion m^3 could differ by up to 178 million m^3. Finally, it was shown that according to mapping objectives, the type of inversion needs to be selected carefully to maximize the use of the highly valuable airborne data.

1. Introduction

Globally, over 600 million people live within low-elevation coastal zones less than 10 m above sea level; this number is estimated to rise to over 1 billion by 2060 (Neumann et al., 2015). As many of these areas are around or below sea level, fresh groundwater resources suffer from saline intrusion—a problem further exacerbated by the threat of sea level rise and land subsidence (Minderhoud et al., 2017; Oude Essink et al., 2010; van Weert et al., 2009). An accurate understanding of the fresh-saline groundwater distribution is therefore required for effective groundwater management. Nonintrusive airborne electromagnetic (AEM) techniques

offer a rapid and cost-effective method with which to achieve this, in contrast to conventional ground-based techniques that offer limited spatial resolution at the larger regional scales required. AEM systems were initially developed for mineral exploration (Fraser, 1978) and comprise two primary methods: frequency and time domain—differences and capabilities of each are discussed in Steuer et al. (2009). Early AEM programs include mapping the fresh-saline groundwater interface over a small island in the North Sea (Sengpiel & Meiser, 1981), and later a more advanced AEM system was used to map fresh groundwater in Pakistan (Sengpiel and Fluche, 1992). These methods have since been successfully applied for groundwater mapping campaigns across the world (e.g., Auken et al., 2008; Chongo et al., 2015; Fitterman & Deszcz-Pan, 2001; Siemon et al., 2015). In the Netherlands, the technique was used in 2009 over the island of Schouwen-Duivenland (Faneca Sànchez et al., 2012) and again in 2014–2015 covering the entire province of Zeeland (Delsman et al., 2018).

Frequency domain AEM, commonly referred to as helicopter-borne electromagnetics (HEM), operate by transmitting electrical signals from an instrument towed beneath a helicopter called a bird. These signals produce currents in the subsurface, which are in turn detected by receivers. As a result, the system detects electrical conductivity (EC) within the subsurface—which, in the case of hydrogeophysical studies, relates primarily (but not exclusively) to clay content of the lithology and/or the salinity of the groundwater (McNeil, 1980). To obtain useful quantitative data, AEM measurements need to be converted into an EC distribution, and ultimately a groundwater salinity estimate, or to map hydrostratigraphy—this is undertaken using a process called inversion. In AEM mapping programs, a number of inversion algorithms are available for this purpose, which include 1-D methods (Farquharson et al., 2003; Siemon, Auken, et al., 2009; Vignoli et al., 2015) or more complex 2-D (Hermans et al., 2012) and 3-D (Cox et al., 2012; Scheunert et al., 2016) inversions. To validate new inversion techniques (or improvements on existing algorithms), these are typically tested using a synthetic model and then applied to an area where relatively little is known about the subsurface (Auken et al., 2005; Farquharson et al., 2003; Siemon, Auken, et al., 2009). Furthermore, inversions used in applied hydrogeophysical studies are often presented without a sensitivity analysis of the effects of available inversion types and inversion parameter settings. Using a probabilistic approach, Minsley (2011) illustrated that a range of inversion models can sufficiently explain the measured frequency domain (or observed) data, highlighting the problem of accepting a single result that *fits*. As academia has observed a year-by-year increase in hydrogeophysical related publications (Binley et al., 2015), it is therefore suggested that the uncertainty introduced by the inversion process on estimated resistivity and derived subsurface properties, including salinity, should be better understood. A comparison of inversions was undertaken by Hodges and Siemon (2008), qualitatively comparing the capabilities of a number of 1-D techniques by means of a synthetic model and real data using two flightlines. This article aims to build on this by quantitatively examining the practical effectiveness and uncertainty of a number of frequently used 1-D inversion algorithms, while making use of 2-D sections and interpolated 3-D models. This is possible due to extensively available HEM and ground data in the province of Zeeland, the Netherlands, where the subsurface distribution of geological and hydrological features is thoroughly understood.

In the following, some of the most commonly used 1-D inversion methods used for AEM were first tested individually for different inversion parameter settings using a test flightline. Second, based on these results, four different inversion methods were selected for further analysis, where remaining flightlines were inverted for each. Third, results were interpolated into 3-D volumes of EC and transformed into groundwater EC using geological information. Finally, inversion uncertainty was analyzed based on practical hydrogeophysical mapping aims, such as groundwater salinity distributions and groundwater interface mapping. Section 2 introduces the study area and available data, with an overview of inversion methods. Section 3 presents the methods and the selection process for inversion parameter settings, followed by the results in section 4 and a discussion in section 5.

2. Background

2.1. Study Area

Located in southeastern Netherlands within the province of Zeeland, the rhombic-shaped former island of Walcheren (~20 × 20 km^2) faces the southern North Sea (Figure 1). Along the coast, topography is characterized by elevated sand dunes—reaching a height of around 40 m above sea level. Inland, the so-called *creek*

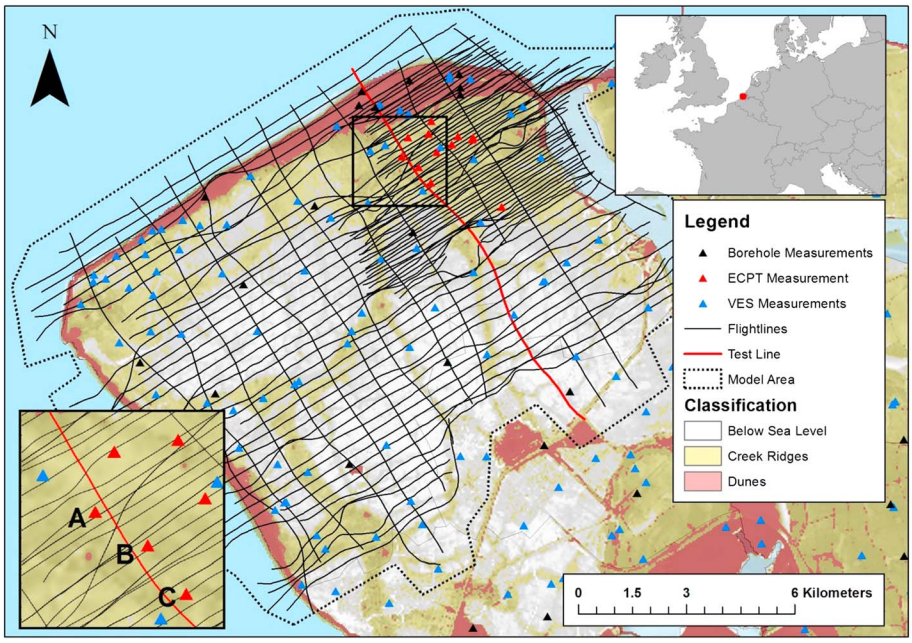

Figure 1. The 2-D horizontal map of the study area, including flightline locations (thin black lines), the test line location (thick red line), ground data (red) triangle: ECPT, black triangle: boreholes, and blue triangle: VES. Dune areas (red) and creek ridges (yellow). Zoomed area highlights labeled ECPT used for analysis. ECPT = Electric Cone Penetration Test; VES = Vertical Electrical Sounding.

ridges are apparent. They are the result of topographic inversion by agricultural drainage, which resulted in a larger subsidence of the adjacent peat-dominated low-lying polders than of the former sandy tidal creeks (Pauw et al., 2015). Much of the rest of Walcheren lies at, or below sea level.

2.2. Geology

Geologically, Walcheren is located at the southern edge of the North Sea basin and comprises gently north dipping Neogene and Quaternary sediments (Stafleu et al., 2011). As a result of sequential sea level transgressions throughout the Holocene, these sediments were deposited mostly in shallow marine, estuarine or fluvial conditions (Vos, 2015). Holocene sediments primarily comprise the Naaldwijk formation—consisting of the Wormer and Walcheren members that lie above an eroded peat unit called the Basisveen. The Wormer member is heterogeneous and comprises fine sands and clay. The surficial Walcheren member is separated from the Wormer by a thick peat unit and consists of 1- to 5-m thick clay-rich tidal flats, sand-rich tidal channels that caused up to 45-m deep incisions into the underlying sediments. Along the coast, the Zandvoort and Schoorl members of the Naaldwijk formation form a sandy coastal barrier (Stafleu et al., 2011). The underlying Pleistocene deposits include the sands and silts of the periglacial Boxtel formation deposits, which have in places been eroded by the Walcheren member tidal channels.

2.3. Hydrogeology

A current estimate of the fresh-brackish-saline groundwater distribution has been recently undertaken across the Dutch province of Zeeland using the HEM data available for this study (Delsman et al., 2018; Van Baaren et al., 2018). The hydrological situation of Walcheren is largely influenced by early Holocene sea level transgressions and the subsequent construction of man-made coastal defenses (Berendsen, 2005). Sea level transgressions during the Holocene caused extensive salinization, whereby the denser saline water displaced the less dense freshwater in shallow aquifers (Delsman et al., 2014). The construction of coastal defenses and resulting land reclamation prevented further sea water inundation and in turn allowed the freshening of shallow aquifers. Freshening primarily occurs through the formation of rainwater lenses, where less dense fresh groundwater *floats* on the underlying denser saline groundwater (Goes et al., 2009). In Walcheren, this lensing effect is observed differently in three main areas: (1) 2-m thick lenses in low-lying areas, (2) 5- to 15-m thick lenses underneath creek ridges, and (3) up to ~60-m thick around coastal dunes (Delsman et al., 2018).

Table 1
Data Types and Quantities Used in This Study

Name	Type	Quantity
Helicopter-borne EM (HEM)	Airborne geophysical	~1,000-line kilometers
Electrical Cone Penetration Tests (ECPT)	Ground geophysical	12 holes
Geo-electrical boreholes	Ground geophysical	16 holes
GeoTOP	Ground geological; 3-D geological model	From surface down to 50-m depth
Vertical Electrical Sounding (VES)	Ground geophysical	~80 measurements

Note. EM = electromagnetics.

As freshwater lens thicknesses are controlled by geomorphological features (Goes et al., 2009), they are easily identifiable using topographical data, as observed in Figure 1.

2.4. Data

The available geophysical and geological data in Walcheren are summarized in Table 1 and illustrated in Figure 1. The data are described in more detail in the following section.

2.4.1. HEM Survey

In 2014/2015 a HEM survey was flown over the entire province of Zeeland, the Netherlands, by the Federal Institute for Geosciences and Natural Resources (BGR). The survey was undertaken for the research project FRESHEM Zeeland (fresh salt groundwater distribution by helicopter electromagnetic survey in the province of Zeeland) and a research program involving Deltares, the Geological Survey of the Netherlands (TNO) and BGR. The survey covered an area of ~2,000 km^2, totaling over 9,000 line kilometers. The primary aim of FRESHEM was to translate the HEM data into a 3-D volume of fresh-saline water distributions in the subsurface (Delsman et al., 2018).

The survey was flown with the following parameters by BGR's RESOLVE System (manufactured by Fugro Airborne Surveys, Table 2).

Over the study area in Walcheren, available airborne data totals ~1,000 line kilometers, covering an area of ~270 km^2—as reading is taken approximately every 4-m downline, in total about 250,000 individual airborne measurements were available. Line spacing was mostly flown at 300 m across most of the area; however, to the north this was decreased to 100 m over an area of interest called the Waterfarm. Tie lines were flown perpendicularly to these at 1,000-m spacing. Flightline orientation was selected to be perpendicular to the strike of prominent features such as dunes and creek ridges and was therefore oriented NE-SW or NW-SE for tie lines. As inversion results directly depend on data quality, AEM data requires careful processing to minimize influence from measurements that do not reflect the targeted subsurface properties. This process is summarized as follows: (1) data were calibrated in the field to more accurately convert observed data into parts per million (ppm) relative to the primary field; (2) measurement drift was corrected during the survey and post-processing; (3) microleveling was applied to remove striping in the data; and finally, (4) based on a data quality assessment, selected data were removed—such as those affected by man-made infrastructure or where the altitude of the HEM system was increased for safety reasons. Detailed reviews and processing steps undertaken for HEM surveys are available in Siemon et al. (2011).

Table 2
Instrument Parameters and Specifications Used by BGR for the HEM Survey

Towed bird HEM system specifications	
Frequencies	380, 1770, 5410, 8300, 41000, and 129500 Hz
Coil separation	~8 m/9 m (depending on conductivity)
Coil orientations	5 × horizontal coplanar, 1 × vertical coaxial
Depth of investigation	50–150 m max
Measurement spacing	~4-m downline
Bird type and manufacturer	RESOLVE, BKS60. Fugro Airborne Systems
Survey parameters	
Flightline spacing	300 m (100 or 200 m in some areas)
Bird height	~40 m

Note. BGR = Geosciences and Natural Resources; HEM = helicopter-borne electromagnetics.

BGR's RESOLVE HEM system generates primary magnetic dipole fields through transmitter coils, which in turn induce eddy currents in the subsurface. The coils are housed in a *cigar*-shaped instrument towed beneath a helicopter called a bird, which typically is about 10-m long. Each of the transmitter coils produces sinusoidally varying currents at discrete frequencies, ranging from 380 Hz to 130 kHz. Low and high frequencies relate to deep and shallow features, respectively. The eddy currents generate secondary magnetic fields based on the conductivity distribution of the subsurface, which are measured by receiver coils. Due to the induction process within the Earth, there is a small phase shift between the

primary and secondary field, that is, the relative secondary magnetic field is a complex quantity having in-phase (*I*) and quadrature (*Q*) components. The measured secondary field is very weak compared to the primary. Therefore, the primary field is *bucked out* and receiver coils record the data in parts per million relative to the primary field. Coil orientation is selected according to survey requirements and is either vertical (VMD: vertical magnetic dipole) or horizontal (HMD: horizontal magnetic dipole); corresponding receiver coil orientation is coupled to that of the transmitter. The system's depth of investigation (DOI) ranges approximately from 50 to 150 m in conductive or resistive conditions respectively. A more detailed review and description of the RESOLVE system are available in Siemon, Christiansen, et al. (2009).

2.4.2. Electric Cone Penetration Test

Twelve Electric Cone Penetration Test (ECPT) measurements were used for this study, all located in the densely sampled area called the Waterfarm. These were mostly measured at, or adjacent to creek ridges. Data were sampled vertically every 0.5 cm up to a depth of around 25 m below surface. Originally developed for geotechnical surveys, cone penetration testing (CPT) forces a cone-shaped tool vertically into the ground at a controlled rate, whereby resistance and friction are measured to obtain a vertical soil profile (Begemann, 1965). With the addition of an EC sensor (henceforth ECPT), a profile of EC is measured. ECPT has been used extensively as a high vertical resolution tool for hydrological mapping purposes (De Louw et al., 2011; Gunnink et al., 2012).

2.4.3. Boreholes.

Located throughout the study area, 15 geo-electrical borehole measurements were available. Importantly, a number of these were measured to a greater depth in the dunes areas to the north, where a deeper fresh-brackish groundwater interface is expected. Measurement depths range from 10 m in the central area to ~45 m in the coastal dune areas. The method works by using an electrical probe, where a measurement is taken every 5 cm and measures conductivity of both the groundwater and lithology and, therefore as with ECPT data, measures bulk EC. A detailed description of the method is available in Spies (1996).

2.4.4. Geological Data

The Geological survey of the Netherlands (TNO) hosts a national database of geological data and models (dinoloket.nl—accessed November 2016). TNO's GeoTOP provides a high-resolution 3-D volume of the onshore part of the Netherlands up to 50-m depth. Available as a 3-D voxel model, the volume contains numerous properties for each cell at a horizontal and vertical resolution of 100 and 0.5 m, respectively. Properties used for this study were lithoclasses, where an estimate of the following classes was available for each cell: peat, clay, sandy clay and clayey sand, fine sand, medium-grained sand, coarse-grained sand, and gravel. A more detailed description of the geological model and how it was constructed is available in Stafleu et al. (2011).

2.5. Geophysical Inversions

Geophysical inversions calculate a distribution of physical properties based on a set of observations or measured data. In electromagnetics, this is fitting a calculated electromagnetic response to a set of observed values. The resulting physical properties can be presented in SI units as either conductivity in Siemens per meter (S/m) or the reciprocal—resistivity in ohm-meter (Ω m). For consistency, conductivity as S/m will be used to present results and describe data in this paper. In order to delineate features in the subsurface, a physical property contrast is required—in the case of EC, these are present as clay content, water saturation, water salinity, and temperature (McNeil, 1980).

As hydrogeophysical investigations are often conducted in areas with young, horizontal or subhorizontal substrata, physical property contrasts are generally horizontally smoothly varying. Furthermore, depending on system altitude, system frequency, and subsurface EC (Tølbøll & Christensen, 2007), HEM systems have a relatively small footprint (~100–200 m); therefore, the benefits of 2-D (e.g., Boesen et al., 2018; Li et al., 2016) and 3-D (e.g., Cox et al., 2012; Scheunert et al., 2016) inversions are limited and considered to be impractical compared to the less computationally expensive 1-D techniques. As a result, this study will focus on 1-D inversion methods only. A number of these are available for HEM (e.g., Auken & Christiansen, 2004; Brodie & Sambridge, 2006; Farquharson et al., 2003; Huang & Fraser, 1996; Macnae et al., 1998; Siemon, Auken, et al., 2009; Viezzoli et al., 2008; Vignoli et al., 2015; Yin & Hodges, 2007). However, for practical purposes, it was decided that a thorough analysis of all available 1-D methods was not possible. Instead, a

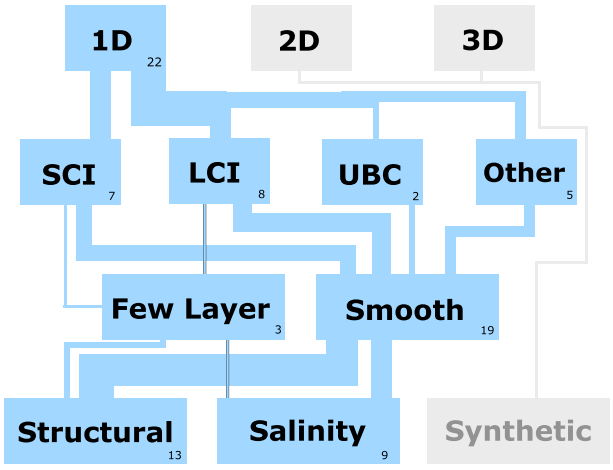

Figure 2. Results of a literature review studying commonly used inversion techniques and mapping objectives. SCI = spatially constrained inversion, LCI = laterally constrained inversion, UBC =University of British Columbia EM1DFM. *Other* refers to studies that were either unclearly specified or used other older methods such as homogeneous half-space inversions. Structural = mapping of hydrological units. Salinity = mapping of saline distributions or salinity interfaces. (Auken et al., 2008; Ball et al., 2010; Bedrosian et al., 2013; Brodie et al., 2004; Chongo et al., 2015; De Louw et al., 2011; Delsman et al., 2018; Faneca Sànchez et al., 2012; Fitterman & Deszcz-Pan, 2004; Gunnink et al., 2012; Haider et al., 2014; He et al., 2014; Herckenrath et al., 2013; Hill, 2011; Jørgensen et al., 2012; Rasmussen et al., 2013; Sengpiel and Fluche, 1992; Siemon, Auken, et al., 2009; Siemon, Christiansen, et al., 2009; Siemon et al., 2015; Wynn, 2005).

literature review of applied AEM-based hydrogeophysical studies was undertaken in order to highlight the most commonly used methods. Results of this are presented in Figure 2.

Here it was found that over ~50% used either laterally constrained inversion (LCI) or University of British Columbia (UBC) EM1DFM (Farquharson et al., 2003) inversions, while another ~30% used the spatially constrained inversion (SCI) method (Auken & Christiansen, 2004; Viezzoli et al., 2008). The SCI process requires a number of neighboring lines to be inverted in order to test measurements along a single flightline, a process that is further complicated because the regularization term needs to be selected according to flightline spacing—where the Waterfarm area has a line spacing of 100 m, in contrast to the 300-m spacing flown for remainder of Walcheren. It was therefore decided that a robust analysis of SCI was impractical for this study.

Both LCI and EM1DFM inversion methods recover a layered, discretized model of the subsurface, where a distribution of EC and corresponding depths are recovered—known as 1-D layered half-space inversions (Sengpiel & Siemon, 2000). Here these inversion algorithms will be subcategorized into two types: (1) smooth, multilayer inversions (Constable, 1987; Farquharson et al., 2003) and (2) layered, few layer inversions (Auken & Christiansen, 2004). Smooth, multilayer inversions (Type 1) have fixed thicknesses, whereby the starting model layer thicknesses are preserved. Layered, few layer inversions (Type 2) invert for both layer thicknesses and conductivity values and have between three and nine layers. Both types take all frequencies into account. Multilayer (Type 1) inversions aim to produce smooth, minimum structure models that lack sharp boundary definition, whereby the smoothest model that fits the data is sought (Farquharson et al., 2003). In contrast, few layer (Type 2) inversions result in sharp boundaries as a result of the inclusion of depths as a parameter and are therefore suitable for areas with more horizontally continuous formation boundaries (Auken & Christiansen, 2004).

In these inversions, there are generally more unknowns than observed data, resulting in an infinite number of possible outcomes, otherwise known as nonuniqueness. In mathematics this is referred to as an ill-posed or underdetermined problem (Tikhonov & Arsenin, 1979). These algorithms therefore need stabilization, otherwise known as regularization (e.g., Constable, 1987; Marquardt, 1963). Regularization is introduced through the model norm, which favors specific properties in the inverted model. The balance between fitting the data and the regularization is approached as an optimization problem—conceptually, this can be expressed as minimizing the objective function (Farquharson & Oldenburg, 2004):

$$\phi(m,p) = \phi_d(m,p) + \beta\phi_r(p) \tag{1}$$

where the vector p contains parameters of the Earth model, m is a vector with the observed data, ϕ_d is data misfit, ϕ_r is a regularization term based on the difference between current parameter values and the initial estimate of the parameters of the Earth model, and β is the regularization parameter that balances ϕ_d and ϕ_r. If the data are fitted too well, artifacts could be present in the final model, resulting in unrealistic structures. Conversely, a fit too far from observed data will result in a model that opts to fit data according to the regularization term used instead. This effect is generally referred to as a trade-off, whereby the regularization term can be set to be fixed if noise levels are understood or calculated automatically (Farquharson & Oldenburg, 2004). In smoother, minimum structure methods, a fit that favors the trade-off parameter will result in a smoother model. The addition of lateral and spatial constraints used in LCI and SCI methods allows the adjustment of the inversion input parameter to favor proximity to neighboring models (Auken & Christiansen, 2004; Viezzoli et al., 2008).

As well as a regularization term, layered half-space inversions require a conceptualized model of the subsurface, or a starting model, where the Earth is discretized into a set number of layers, each of which are given

property and thickness values. Starting models can be based on prior knowledge, such as known (hydro) geological boundaries (Brodie et al., 2004), or automatically generated based on observed data using sounding curves (Delsman et al., 2018; Gunnink et al., 2012; Sengpiel & Siemon, 2000); mostly, however, these are based on a simplified conceptual model of the subsurface (Auken et al., 2008; Bedrosian et al., 2013; Chongo et al., 2015). The type of inversion, starting model, and inversion parameter settings relating to the regularization term will affect the inversion's outcome. Based on this, the inversion will then iteratively change the starting model until the observed data are sufficiently explained. The response of the current model at each iteration is then calculated by forward modeling and compared to the measured (or observed) data, where a misfit is calculated. The inversion is performed iteratively through a linearized approximation of the nonlinear forward mapping of the model to the data space (Auken et al., 2005; Menke, 1989). The inversion process stops once it reaches a specified trade-off threshold, that is, minimizing a criterion such as equation (1), or until the maximum specified number of iterations is reached. In order for the resulting inversion model to be considered as a potential candidate of the subsurface, a suitable fit to the data is necessary—referred to here as the misfit between observed and predicted data.

UBC inversions comprise four methods, all of which are smooth, multilayer types, and have the same base formulas. However, each method differs in regard to how the trade-off parameter is dealt with (Farquharson et al., 2003; Farquharson & Oldenburg, 2004). These encompass the following: (1) Generalized Cross Validation (GCV), (2) *L* curve, (3) Fixed Trade-Off, and (4) Line Search (Farquharson & Oldenburg, 2004) and will be described in more detail in that order. By searching for a model that is least affected by any other data point, the GCV method provides an estimated value of the trade-off parameter that sufficiently explains the data. As a result, an estimation of noise is provided (Haber & Oldenburg, 2000). For the *L*-curve method, if an inversion misfit is plotted against the model norm for a selection of appropriate trade-off values, an *L*-shaped curve is produced. Here the point of maximum curvature approximately depicts a balance between misfit and model norm and is therefore considered an appropriate trade-off value (Farquharson & Oldenburg, 2004). In contrast to GCV and *L*-Curve methods, Fixed Trade-Off and Line Search methods require an inversion input parameter that assumes some knowledge of noise. The Fixed Trade-Off method is the simplest approach, where the user provides a value that remains fixed throughout the inversion. As a result, this method has the fastest calculation times. It may, however, require a time-consuming trial-and-error approach. As the GCV method results in a determination of trade-off values along a flightline, these could be used as values for the Fixed Trade-Off method. The Line Search approach is most useful if the noise in a set of observation is understood. Here the expectation of the misfit equals the number of observations, and the trade-off parameter is chosen according to a target misfit in relation to this (Farquharson & Oldenburg, 2004). A more technical description of regularization estimation for UBC EM1DFM inversions is available in Farquharson and Oldenburg (2004).

Conceptually, the LCI method consists of linked 1-D models along individual flightlines, where the model spacing is determined by downline measurement spacing. As a result, the models are inverted as one system along each flightline (Auken et al., 2005). LCI inversion input parameters (or trade-off parameters) impose lateral and vertical constraints that tie together resistivities and depths of adjacent layers (Auken et al., 2005). As a result, LCI inversions favor laterally continuous physical property distributions, as demonstrated in Hodges and Siemon (2008). The primary inversion parameters are therefore resistivities, or in the case of few layer methods—also depths, as demonstrated in Figure 3 (adapted from Auken et al., 2005).

Furthermore, LCI inversions allow a sharp option, whereby vertical resistivity changes are permitted to change more rapidly and could be seen as a compromise between few layer and smooth inversions (Vignoli et al., 2015). LCI inversion input parameters are described in detail by Auken et al. (2005) and Vignoli et al. (2015) and will be described and analyzed here as three primary options: (1) horizontal (2) vertical, and (3) sharpness constraints. These inversion input parameters may be chosen based on knowledge of the subsurface, for example, over Walcheren we know that rapid vertical changes in EC are expected within the scale of a few meters, due to expected fresh-saline groundwater interfaces (Delsman et al., 2018). Horizontal variations are expected to be smoother, in the order of around 10 m, due to gently dipping Holocene and Pleistocene sediments (De Louw et al., 2011; Vos, 2015).

In order to effectively assess inversion uncertainty, a misfit threshold between observed and predicted data is needed. This allows differences between the methods and inversion input parameters to be analyzed with

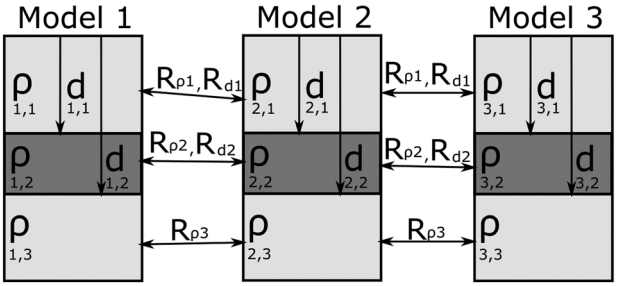

Figure 3. A conceptual figure of the LCI method demonstrating how neighboring models are linked. R = lateral constraints, ρ = resistivity values, and d = depth values. The LCI few layer approach links both depths (d) and resistivities (ρ); the LCI multilayer method links only resistivities (Auken et al., 2005). LCI = laterally constrained inversion.

the knowledge that they fit the data and thus are all *correct*, where each quantitatively represents a possible model of the subsurface. Although the data for this study is of high quality and undergone extensive processing (Delsman et al., 2018), field data will nevertheless always be contaminated with some degree of noise (Siemon, Auken, et al., 2009). As a result, flexibility in regard to misfit is required, where an estimate of noise can inform the threshold misfit value for inversion results. For this study an approximate value of 5% will be used based on previous estimates (Farquharson et al., 2003), and therefore, in this paper results that do not fit this criterion will be excluded. In the following, misfit is calculated as relative %, using the method of Siemon, Auken, et al. (2009).

3. Methodology

Inversions were undertaken using two platforms: (1) UBC's EM1DFM code through the UBC Geophysical Inversion Facility (UBC GIF, Farquharson et al., 2003) and (2) LCI inversion methods using Aarhus Workbench (Auken & Christiansen, 2004; Vignoli et al., 2015). Initially, eight separate inversion types were tested using a single flightline, encompassing each of the four EM1DFM trade-off options, two LCI multilayer inversions, the *smooth* and *sharp* inversions, and the few layer LCI method with either five or nine layers.

The process is summarized by an eight-part workflow as illustrated in Figure 4 and discussed in order in sections 3.1 to 3.8.

3.1. Processing of HEM Data

Standard processing of the HEM data was undertaken by BGR and, for this survey, is summarized in Delsman et al. (2018) and detailed in section 2.4.1. The following postprocessing steps were undertaken for this study: (1) measurements where bird altitudes above 60 m were removed due to low signal to noise ratios, and (2) every second downline measurement was removed, resulting in a measurement every 8 m to facilitate faster inversion times. As the footprint of the HEM system is ~100 m to 200 m (Tølbøll & Christensen, 2007), an 8-m measurement distance is assumed to have no or little effect on the outcome, while allowing practical computation times given the amount of inversion runs required for this study.

3.2. Inversion Setup

All data were inverted using measured in-phase (I) and quadrature (Q) secondary field data. To minimize ambiguity, it was decided that the same starting model was to be used for all inversions. For smooth and sharp multilayer inversions, these were chosen to consist of 20 layers, with the thickness of the top layer starting at 0.5 m and subsequent layers increasing logarithmically with depth till 60 m. These layers are parallel to Dutch AHN25 topography data, a high-resolution LIDAR topographical data set of the Netherlands. For few layer inversions, the same criteria were applied but using 5 layers instead of 20. The 60-m depth was chosen according to borehole measurements in the dune areas, where they indicated a probable fresh-saline groundwater interface at a maximum depth of ~50 m, based on observed strong conductivity contrasts. This depth also reflects the DOI capabilities of the HEM system. For inversions undertaken in Aarhus Workbench, a starting conductivity of 1 S/m was selected owing to the highly conductive saline environment

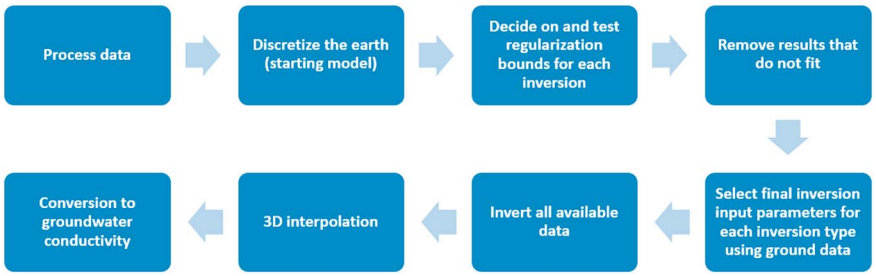

Figure 4. The eight-part methodology workflow used for this study.

Table 3
Parameter Sets Tested Along With Descriptions and Ranges to be Used

Inversion name	Parameter name	Description	Ranges	Reference
UBC fixed trade	Trade-off	Trade-off value	0.5–3	Farquharson and
All UBC Inversions	Decrease	Greatest allowed decrease in the trade-off parameter per iteration	0.011–1	Oldenburg (2004)
UBC line search	Chifact	Trade off value	0.5–10	
LCI smooth	Later/Vertical Constraints	Amount that neighboring constraints can change. A higher numerical allows more change and vice versa.	Lateral: 1–3, vertical: 1.5–3	Auken et al. (2005)
LCI sharp	Sharp numeric	Vertical and horizontal sharpness of the model	Vertical: 1–100, horizontal: 1.5–150	Vignoli et al. (2015)

Note. UBC = University of British Columbia; LCI = laterally constrained inversion.

of Walcheren. For UBC inversions, the starting conductivity was calculated automatically for each inversion as this was found to improve stability, particularly in areas where apparent shallow, highly conductive features were present (Farquharson & Oldenburg, 2004).

3.3. Regularization Parameter Choices

For practical purposes, inversion types and parameter inputs were initially tested on a single flightline. Flightline 9.9 (Figure 1) was selected for this purpose, as it covers a range of hydrological settings, including a shallow, highly conductive area to the south-east, and crosses perpendicularly to the more resistive dune area to the north-west. It was also found that bird altitudes were relatively high in some places, likely because of proximity to anthropogenic features, and therefore offers a range of mapping challenges, many of which would typically be found in a HEM survey. Furthermore, this flightline is in close proximity to available ground constraints. Inversion parameter input options for each inversion type are summarized in Table 3, alongside the ranges of values used for this study. For each inversion method, a significant number of parameter input combinations are possible; therefore, parameter values were changed one parameter at the time, while keeping the other parameters at their defaults (ceteris paribus). In total over 70 separate inversions were run for this process.

Initial upper and lower bounds for inversion parameter settings were decided on practical criteria such as inversion stability, observing data misfit and previously used values in published literature (Bedrosian et al., 2016; Gunnink et al., 2012).

3.4. Removing Inversions Results From Further Analysis

Out of the initial ~70 inversion runs, a subset of ~25 was selected for further analysis. Inversions were removed for one of three reasons: (1) a noticeable change in the inversion outcomes was not observed (i.e., adjusting the inversion input parameter resulted in almost no difference compared to the next inversion and therefore, for practical reasons, was not included in the analysis); (2) results showed apparent instability, and (3) the inversion did not converge to within the 5% misfit threshold and therefore was excluded as a potential candidate of the subsurface. Figure 5 shows observed and predicted data for a LCI smooth inversion result, where misfits are in the 1–3% range; misfit plots for the other three inversions are available as supporting information.

Out of the four UBC trade-off options, the Fixed Trade-Off inversion was consistently more stable and converged successfully. It was therefore decided to only use the UBC Fixed-Trade method for further analysis; however, the GCV was useful at suggesting an appropriate inversion input parameter. The 9 layers used in the LCI few layer approach were discarded despite successfully converging, as conceptually there are between 5–10 degrees of freedom within the data space (encompassing both in-phase and quadrature components) and 18 parameters in the inversion. Therefore, without prior constraints, the inversion could not be trusted.

As a result of removing inversions based on the criteria above, four methods remain: (1) 20-layer LCI smooth, (2) 20-layer LCI sharp, (3) LCI five layers, and (4) 20-layer UBC fixed trade-off.

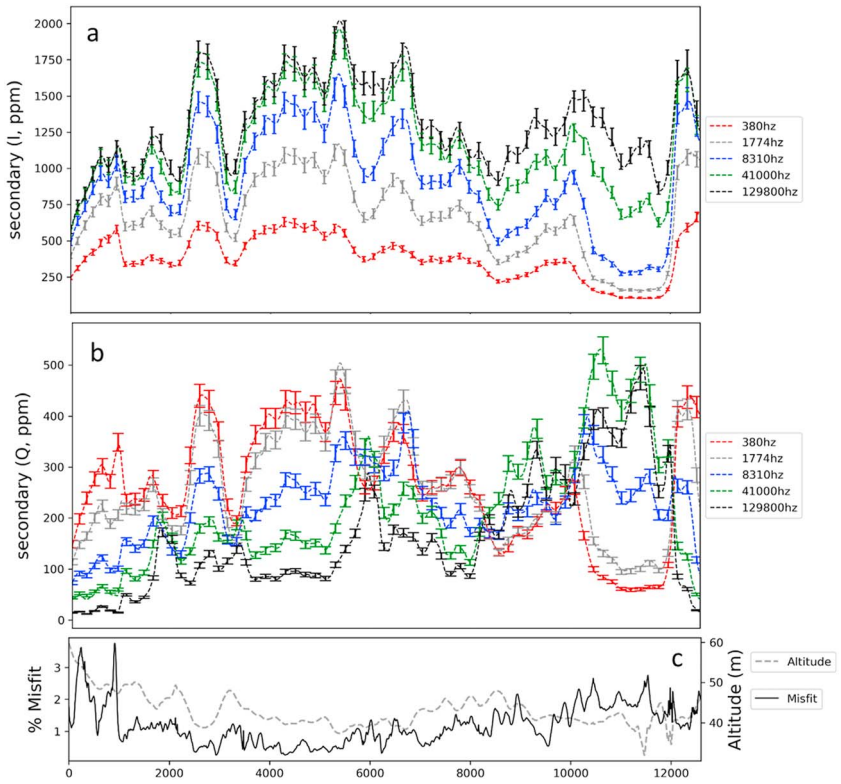

Figure 5. LCI smooth inversion results, lateral and vertical constraints input as 1.3 and 3, respectively. Predicted (dashed lines) and observed (as error bars as 5% of data magnitude) for in-phase (a) and quadrature (b) components. Misfit (c) shown as solid black line as relative % error, and instrument altitude as gray dashed line. LCI = laterally constrained inversion.

3.5. Testing Regularization Terms

In order to the assess the robustness of the remaining four inversion methods with different regularization parameters, 2-D sections of inversion results with standard deviations of conductivity were plotted for each of the regularization parameter sets, along with misfits. The variance plots illustrate areas in the inversion result that showed the largest (or least) change in the inversion outcome by changing the regularization term (or inversion input parameter) between the bounds shown in Table 3. Figure 6 illustrates two examples of this, one from the UBC Fixed Trade parameter and another from the LCI smooth lateral/vertical constraint options. These are plotted with a single inversion result each to assess the overall structure of each model.

3.6. Selecting Inversion Parameters for Each Code

As observed in the variance plots (Figure 6), predictably the inversion parameter settings for each inversion type resulted in easily observable differences, with standard deviations observed at just over 0.1 S/m in some areas. This effect was more prevalent in three groupings: (1) shallow, highly conductive regions on either end of the profile, (2) intermediate zones with distinct linear characteristics, and (3) deeper areas, often at the base of the DOI toward the north-west. For these reasons, final input parameters were selected based on an unbiased quantitative means. This was done by comparing all inversion results to nearby ECPT data. Searching to a maximum distance of 150 m to the test line, three ECPT measurements were used for this purpose (labeled A–C in Figure 1), whereby the 10 nearest 1-D inversion models were averaged for each ECPT location to smooth out single anomalous inversion results. Finally, these were compared directly with one another, where absolute differences were calculated by subtracting ECPT data with each inversion result. To demonstrate the method, results from the LCI smooth parameter (lateral/vertical constraints) set are illustrated in Figure 7.

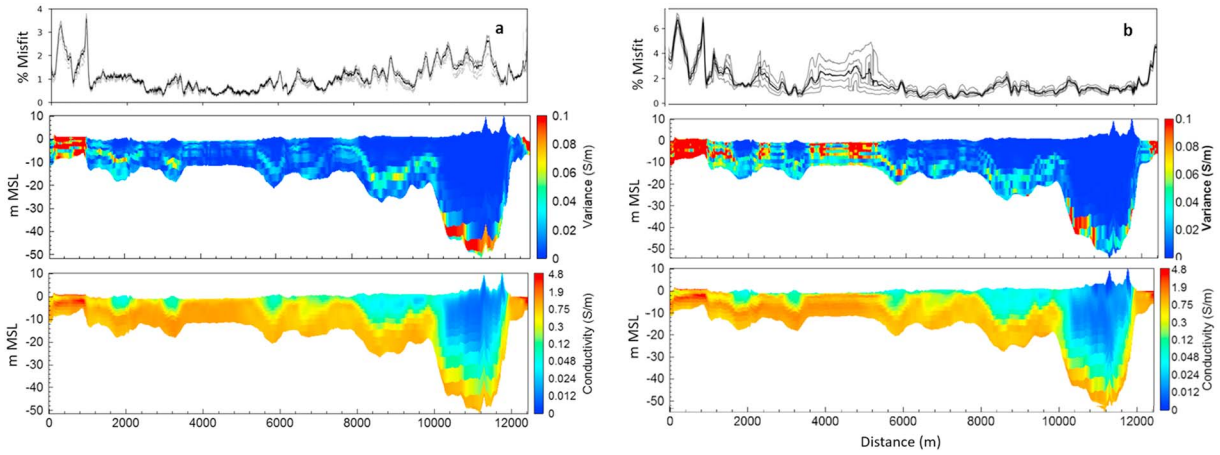

Figure 6. Variance plots testing inversion robustness based on regularization parameters with misfit to observed data. (a) LCI inversion, lateral/vertical constraints variance with inversion result. (b): UBC Fixed Trade variance with inversion plot (Fixed Trade-Off parameter = 2). Misfit is represented relative difference as percentage. The blanked out area is the result of applying the DOI calculation from the LCI smooth result. LCI = laterally constrained inversion; DOI = depth of investigation.

To reduce ambiguity and bias, misfit to each individual ECPT was not analyzed in detail. Rather, the best fitting parameters were selected based on an overall best fit, which is the average difference of each of the three ECPTs. The inversion types and corresponding best fitting regularization parameters for each of the finally selected inversion method are listed in Table 4. On the assumption that these parameters would be best suited for the entire area, these were chosen for further analysis and inversion of the entire data set. The best regularization results from the LCI multilayer inversions were also applied to the few layer inversion.

3.7. 3-D Interpolation

Having a continuous 3-D distribution of properties permits the use of a versatile environment where properties can be analyzed in a 3-D GIS workspace, allowing the undertaking of a comprehensive analysis such as

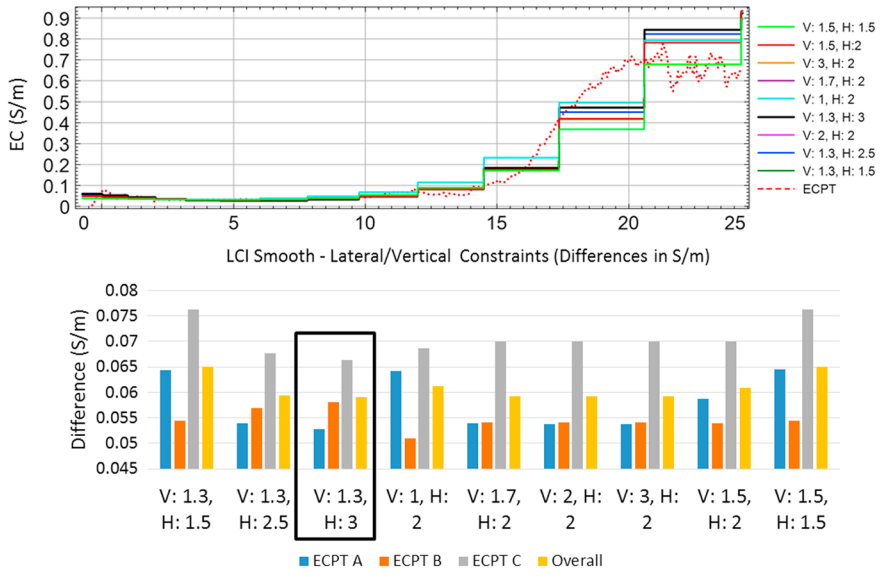

Figure 7. (top) An example vertical section of LCI lateral/vertical constraints input versus ECPT *C* (ECPT locations illustrated in Figure 1), parameter set (V: 1.3 H:3; see Table 3 for an explanation of these parameters) that resulted in a closest match is highlighted in black. (bottom) Mean fit between inversion model EC and ECPT data, final choice highlighted by the black box. Misfit is based on average absolute value mismatch in Siemens per meter. LCI = laterally constrained inversion; ECPT = Electric Cone Penetration Test; EC = electrical conductivity.

Table 4
Final Regularization Parameter Choices Based on a Quantitative Match to ECPT Data on Flightline 9.9

Final inversion parameters	Trade-off	Decrease	Chifact	Lateral and vertical standard deviation	Power law	Vertical and horizontal sharp Numeric
UBC fixed trade	3	0.5	N/A	N/A	N/A	N/A
LCI smooth	N/A	N/A	N/A	L: 1.3, V: 3	1	N/A
LCI sharp	N/A	N/A	N/A	L: 1.3, V: 2	1	V: 30, H: 15
LCI 5 layers	N/A	N/A	N/A	L: 1.3, V: 3	1	N/A

Note. ECPT = Electric Cone Penetration Test; UBC = University of British Columbia; LCI = laterally constrained inversion.

fresh groundwater volume estimates and fresh-brackish groundwater interface depths. This article's focus is on quantitatively comparing inversion algorithms and parameters thereof, rather than interpolation methods. The interpolation method therefore needed to be simple, unambiguous, and consistent, while honoring the following minimum requirements: (1) conform exactly to data directly beneath sounding locations, avoiding excessive smoothing (except for resolution de-sampling); (2) layered nature of the inversions should be maintained with minimal smoothing; (3) resolution of the 3-D model should closely reflect the resolution of the HEM system, while maintaining a reasonably sized model that is not too bulky; and (4) lightweight enough that all four inversions can be practically interpolated and merged into one voxel model.

For these purposes, a method similar to that of Pryet et al. (2011) was selected where the conductivity distribution of each inversion layer is gridded using 2-D horizontal kriging. Using the depth information from starting models (and layer depths of few layer inversions), each 2-D conductivity grid could be *filled* vertically into a 3-D voxel. A 2-D ordinary kriging method as coded in Geosoft's Oasis Montaj was used to interpolate conductivity values, where a spherical semivariogram model was used. A 50-m horizontal resolution was deemed appropriate considering the footprint of the HEM system and also conformed to the resolution of the GeoTOP model (i.e., the lithological model used for formation factor (FF) values; see section 3.8). The resulting grids were saved to a database for each inversion, where depth values for the smooth inversions were added from starting models. For the few layer inversions, the inverted depths were gridded using the same kriging method as above; the resulting grids were then sampled into their respective databases. Finally, the depth values for all inversions were corrected for terrain using AHN 25-m resolution data. With each inversion now saved into a database with *XYZ* coordinates at 50-m horizontal resolution, the data were translated into a 3-D volume. This was done in Paradigm's Gocad, where a $50 \times 50 \times 0.5$-m resolution voxel was created over the study area. As the final layer for each inversion is assumed to be infinitely deep, these properties were filled to approximately twice the thickness of the layer before it. To take into account the penetration depth of the HEM system, the *standard* DOI result from the LCI smooth inversion was applied to the 3-D volume, where values below this depth were removed. For overall consistency, it was decided that the same DOI result was to be applied to all inversions; this includes removing data that were outside of Geotop's geological model, that is, offshore.

The 3-D interpolation result was extensively validated where overall it was found to be appropriate for further analysis and adhered to the initial requirements. A detailed description of the method and validation results are available as supporting information.

3.8. Translating the Conductivity Volume Into Salinity Distributions

Table 5
Apparent Formation Factor (FF) Values Used in This Paper, From De Louw et al. (2011)

Lithology	Formation factor (FF)
Peat	2.1
Clay	2.5
Sandy clay/clayey sand	2.8
Fine sand	3.2
Medium coarse sand	4
Coarse sand	5
Sand with gravel	6–7

In order to interpret the results with respect to groundwater quality, it is necessary to relate the conductivity distribution to that of EC groundwater, rather than simply the conductivity of saturated sediments, or bulk EC. To split the signal, bulk EC is multiplied by the FF, which relates to the lithology, and is primarily a function of pore space and pore connectedness (Archie, 1942). This method is further improved by taking into account factors such as surface conductivity as a result of clay particles (Revil & Glover, 1998). Given that this study examines inversion methods only and therefore does not aim to map salinity directly, it was decided that a simplistic approach was suitable for relative comparisons. An *apparent formation factor* is commonly used for this purpose, whereby the ratio between EC

Table 6
Fresh, Saline, Brackish Classifications for Groundwater EC Used in This Paper, From Paine and Minty (2005)

Conductivities (S/m) or resistivity (Ω m)	Classification
0–0.18 S/m, 0– > 5.6 Ω·m	Fresh
0.18–1.8 S/m, 5.6–0.56 Ω m (0.54 S/m, 1.85 Ω m brackish-saline interface)	Slightly to moderately saline (brackish)
> 1.8 S/m (< 0.56 Ω m)	Very saline to brine (saline)

Note. EC = electrical conductivity.

bulk and EC groundwater based on local observations is utilized (Siemon, Christiansen, et al., 2009). De Louw et al. (2011) collected information from seven different soil types over the Province of Zeeland, including measurements in Walcheren that were found to adequately represent the lithology of the study area. The resulting apparent FF values will be used for this study and are listed in Table 5.

To determine lithology types within the 3-D model, TNO's Geotop model was utilized (Stafleu et al., 2011), where each of the cells within the 3-D model area was assigned with an appropriate apparent FF based on available lithostratigraphic classifications. The FF within the DOI area of the 3-D model was then applied to each inversion result using FF values from individual voxel cells. Finally, using empirical relationships between salinity and EC, it is possible to subdivide the 3-D volumes of groundwater EC into *fresh-brackish-saline* regions, based on the published values listed in Table 6 (Paine & Minty, 2005). All EC values in the following refer to groundwater EC.

Figure 8 illustrates the 3-D result of the LCI smooth inversion, along with some outputs available for analysis.

4. Results

With a 3-D volume of groundwater EC, as well as fresh-brackish-saline regions available for each inversion method, differences between the algorithms were analyzed in novel ways—with a practical and applied

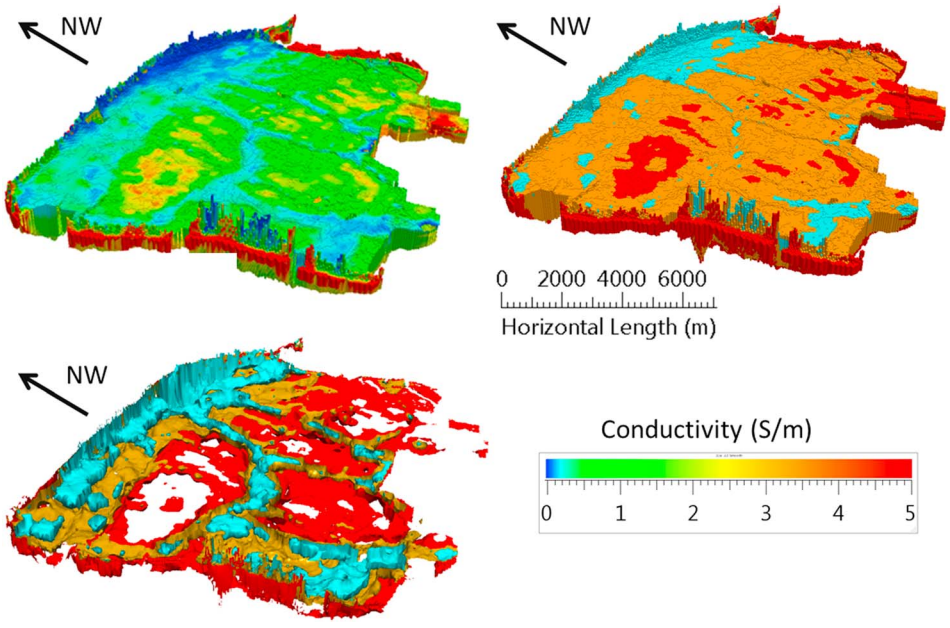

Figure 8. The 3-D interpolation results for the LCI smooth inversion. (top left) EC groundwater (Siemens per meter) low conductivity (blue) and high conductivity (red). (top right) Fresh (blue, < 0.18 S/m), brackish (orange, 0.18–1.8 S/m), and saline (red, > 1.8 S/m) volumes. (bottom left) fresh-brackish (blue, 0.18 S/m), brackish-saline (orange, 0.54 S/m), and saline (red, 1.8 S/m) interfaces extracted as surfaces. Forty times vertical exaggeration. LCI = laterally constrained inversion; EC = electrical conductivity.

focus on some of the mapping requirements for a hydrogeophysical study. Given that the exact same process was explicitly completed for each inversion, and inversion parameter settings were chosen on a quantitative basis, the following assumes that relative differences noted between algorithms are from the inversion method itself. In regard to the use of direct ground measurements, the following should be noted: (1) these are bulk EC measurements and therefore represent the EC of both lithology and groundwater; (2) EC is sensitive to temperature (~2% increase per 1 °C), and (3) no two methods are exactly comparable—thus depending on the conditions of acquisition at the time and method used, EC values will vary. As a result, while the ground measurements are assumed to provide a more accurate (and more localized) measurement of groundwater EC, these are more quantitatively useful as a relative comparison between inversion methods, rather than an exact depiction of a groundwater salinity distribution.

Here results will be presented as follows: (1) qualitative observations; (2) fresh, brackish, and saline groundwater volume estimates; (3) accuracy of salinity distributions; and (4) groundwater interface depth mapping.

4.1. Qualitative Observations

The 3-D model with representative cross sections is shown in Figure 9, comparing LCI smooth, LCI five-layer, and UBC Fixed Trade results to ECPT data. The cross section was designed as irregular in order to illustrate specific features such as *creek ridges* and to intersect ground constraints.

Qualitative comparisons suggest the following: (1) inversions results agreed with each other about the general conductivity distributions, (2) EC contrasts were consistently mapped at around the correct depths, (3) the few layer inversions tended to map a thin resistive layer at the surface, this was less apparent in smooth results, and (4) subtle differences in the amount of structure resolved were observed between the smooth 20-layer results—this is particularly noticeable between the EM1DFM and LCI inversions.

4.2. Volume Estimates

Fresh-brackish-saline volume calculations were completed for each inversion, and the results of which are illustrated in Figure 10. All groundwater volume estimates were calculated as volumes between the AHN25 terrain surface and the base of the DOI. Given that the differences between the terrain surface and the groundwater table are known to be small (Van Baaren et al., 2018), it was decided that using the terrain as an upper boundary was suitable and allowed a straightforward and unambiguous way to compare inversions. As an exact (ideal) 3-D model of the fresh-saline distribution over the study area is unavailable, this quantitative step is useful as a relative comparison only.

Each inversion consistently estimated saline volumes, with a maximum difference of ~4% observed, where salinity volumes were all in the 40% range. Larger differences were noted between fresh and brackish estimates, where the LCI five-layer inversion estimated higher freshwater volumes at ~20%, a difference of ~6.5% when compared with the lowest estimate from the LCI smooth (20 layers) result. Quantitatively, out of a total model volume of 2.8 billion m^3, a freshwater estimate difference of ~178 million m^3 was observed in an area of 20 km × 20 km × ~50 m between the methods. The few layer LCI and LCI sharp inversions favored resolving a smaller brackish (and larger fresh) volume.

4.3. Overall Accuracy of Groundwater Distributions

By transferring the 3-D model EC values to the locations of the ECPT and borehole data, each result could be directly and quantitatively compared. This was achieved by plotting the EC from borehole and ECPT data against the inversions and calculating correlation coefficients for each (Figure 11).

Smoother, multilayer results were consistently closer against both ECPT and borehole measurements. The LCI five-layer inversion correlated the least, compared to LCI smooth that was shown to be overall closer. These are compared in Figure 12.

The cross-plot distributions show that most of the differences are related to the layered nature of the inversions versus the smoothly varying ECPT and borehole data, as observed in Figure 12 by the vertical/horizontal patterns in the LCI five-layer plot.

4.4. Interface Depth Accuracy

Interfaces between fresh-brackish, brackish-saline, and the center of the brackish groundwater zone were extracted from each of the inversion results as isosurfaces, as well as corresponding fresh-brackish-saline

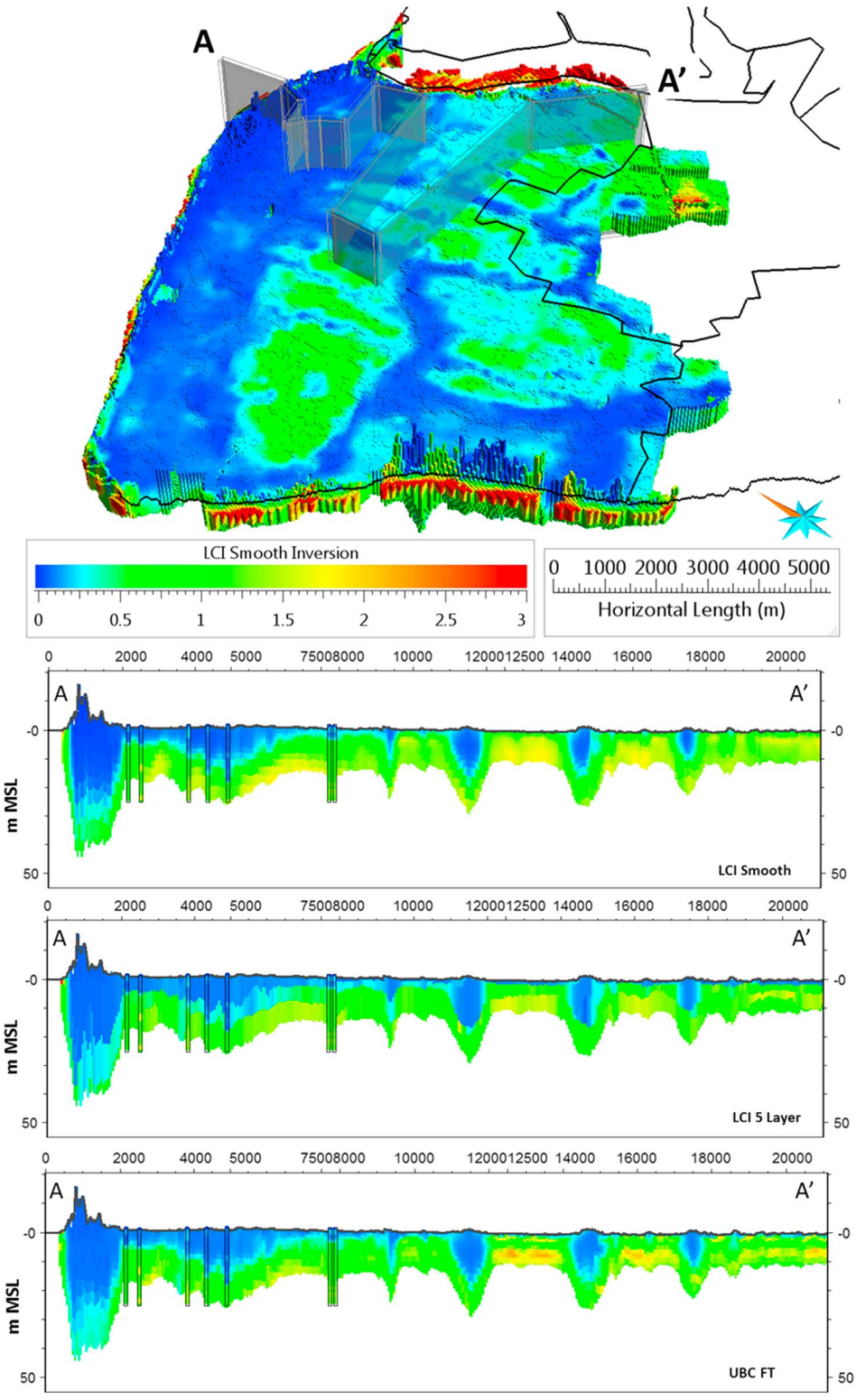

Figure 9. A qualitative view of general inversion result observations. (top) LCI smooth 3-D model with 2-D section locations. (bottom) Results of LCI smooth, LCI five-layer, and UBC Fixed Trade inversions. Forty times vertical exaggeration. Colored by conductivity in Siemens per meter, same color legend for both 3-D models and 2-D profiles. ECPT data highlighted with black outlines. LCI = laterally constrained inversion; ECPT = Electric Cone Penetration Test; UBC = University of British Columbia.

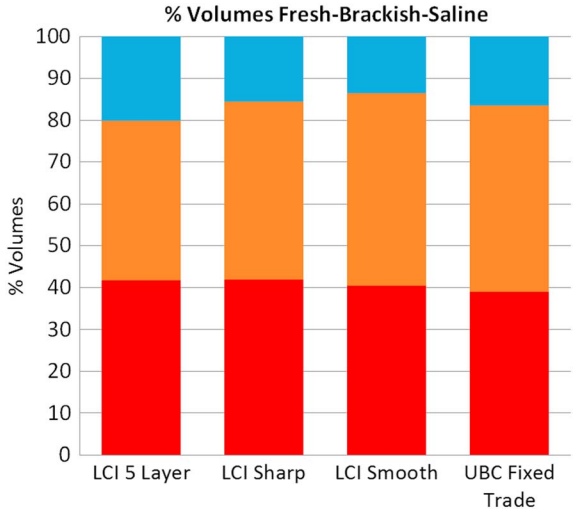

Figure 10. Volume estimates for each inversion. Red (saline, ≥ 1.8 S/m), orange (brackish, 0.18–1.8 S/m), and blue (fresh, ≤ 0.18 S/m). LCI = laterally constrained inversion; UBC = University of British Columbia.

interface depths from ECPT and borehole measurements using groundwater EC values. Figure 13 illustrates the depth to the brackish zone from the LCI smooth result, as well as the 3-D surface with extracted ECPT point values for the brackish interval. For consistency interfaces are presented as fresh-brackish (0.18 S/m), center of brackish (0.54 S/m), and brackish-saline (1.8 S/m), which are based on values listed in Table 6.

Distances from the ECPT and borehole point data to the corresponding 3-D surfaces were calculated as a vertical misfit as both absolute (Figure 14) and ± values (Figure 15); negative values correspond to inversions that were deeper than ground data and vice-versa. As the borehole measurements were often deeper than the ECPT, the two are plotted separately.

From the absolute value misfits in Figure 14, it follows that all methods consistently mapped interfaces within an accuracy range of around 3–4 m against both ECPT and borehole measurements. Furthermore, both comparisons suggest that all inversions were better at resolving the center of the brackish zone (0.54 S/m). Overall, smoother, multilayer inversions were consistent with one another compared with ECPT data. A distinction between the methods is noted in the ECPT misfit, where the fresh-brackish groundwater interface was mapped with greater accuracy by the few layer LCI, multi-layer LCI sharp, and UBC Fixed Trade inversions. This is a mapping error difference of just over 2 m between the inversions. Overall, ECPT misfit suggests that fresh groundwater interface mapping in Zeeland area favors *sharper* techniques; however, less distinction is noted when trying to resolve the center of the brackish zone or the brackish-saline groundwater interface. In contrast to ECPT differences, the deeper borehole measurements suggest that the few layer inversion was less effective at resolving the fresh-brackish groundwater interface, however slightly more accurate in terms of mapping the center of the brackish zone overall.

In order to quantify vertical offset between interfaces and ground data, the above misfits are illustrated as ± values in Figure 15.

Similar patterns are observed in Figure 14, where ECPT data show that the brackish interface was seen to be the most consistently mapped (~ + 2 m ± 2 m), although borehole data suggest that the saline interface was most accurately resolved at the correct offset (~ + 0.5 m ± 4 m). The few layer method more accurately resolved the offset of the fresh-brackish interface compared with the ECPT (~1–2 ± 2 m) and the center of

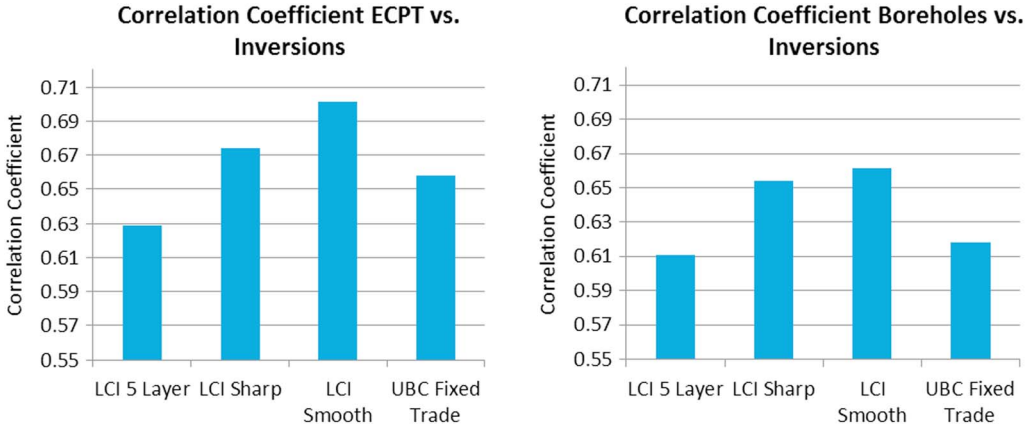

Figure 11. Correlation coefficients based on *XY* plots of each inversion versus ECPT data. (left) Borehole correlation. (right) ECPT correlation. ECPT = Electric Cone Penetration Test; LCI = laterally constrained inversion; UBC = University of British Columbia.

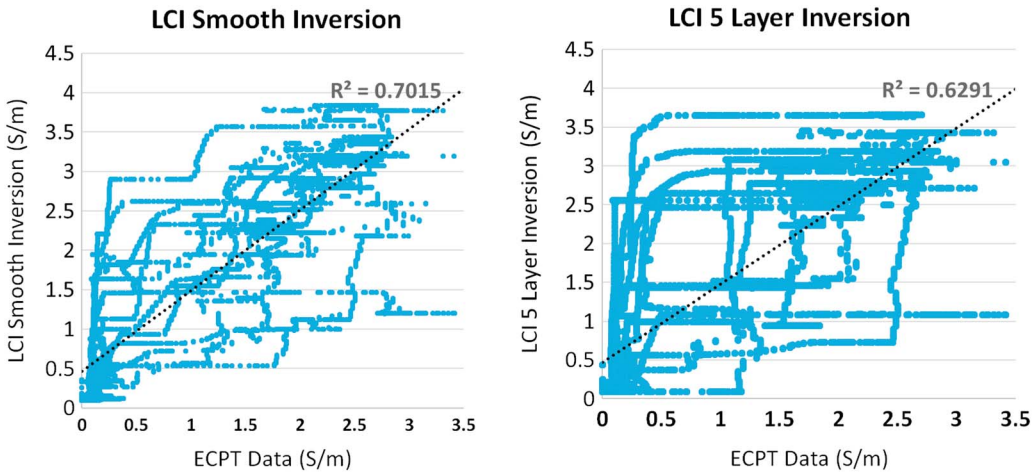

Figure 12. Illustrative *XY* plots based on inversion results versus ECPT data. (left) LCI smooth inversion result. (right) LCI five-layer inversion result. ECPT = Electric Cone Penetration Test; LCI = laterally constrained inversion.

the brackish zone with the deeper boreholes (−1 m to −2 ± 4 m). A constant offset was observed against the ECPT data, whereby inversion results were all around 2 m shallower than predicted. In the borehole data little offset is observed with the saline interface, although both brackish and fresh interface results suggest that inversions were generally deeper.

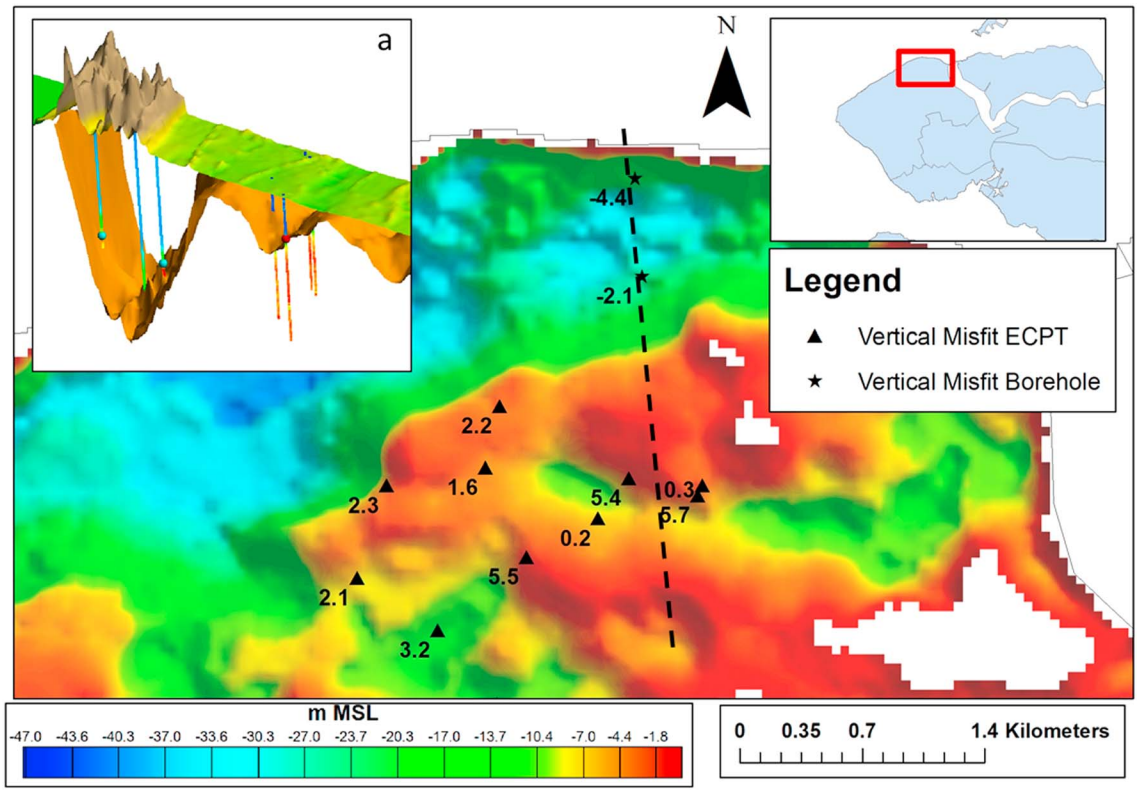

Figure 13. LCI smooth interface mapping result of the brackish interface (0.54 S/m). Black stars (ECPT misfit, meters), black triangles (borehole misfit, meters); misfit is presented as ± values. Background image is colored in depth to the interface with linear color stretch. The black dotted plane is the location of the 3-D inset (a), here red and blue dots show the interface depth extracted from ECPT and borehole data, respectively. ECPT = Electric Cone Penetration Test; LCI = laterally constrained inversion; UBC = University of British Columbia.

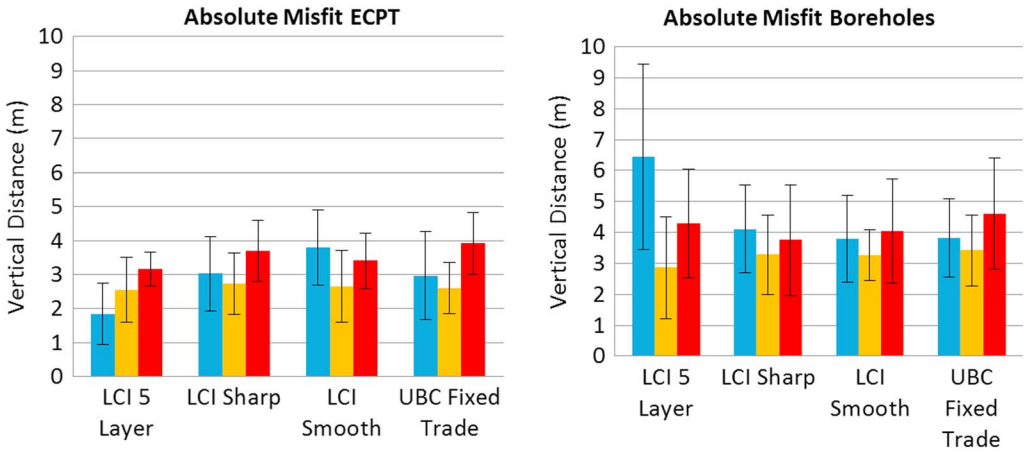

Figure 14. Vertical mismatch (mean absolute differences between observed data) of inversion results to extracted interfaces in meters. Red (saline misfit, 1.8 S/m), orange (brackish misfit, 0.54 S/m), and blue (fresh misfit, 0.18 S/m). ECPT = Electric Cone Penetration Test; LCI = laterally constrained inversion; UBC = University of British Columbia.

5. Discussion

Based on the qualitative results presented in Figure 9, all inversion results are roughly consistent and visually honor the ground data in terms of groundwater EC distributions and locations of major conductivity contrasts. As expected, more obvious differences are observed between few layer and smooth, multilayer methods. Other aspects are more subtle and thus will be discussed here in the same order as section 4. Observations from the variance plots (Figure 6) showed that shallow, highly conductive features were mapped with greater stability by the LCI algorithm. Here a feature between 4 and 5 km showed much greater variability in regard to misfit and resolved features. This is likely because the LCI algorithm was improved to handle high-frequency data found on the Resolve HEM system (Siemon, 2012). It should be noted in the following that the effect of geology in the study area was observed to be relatively insignificant, whereby an obvious and consistent long-wavelength conductivity contrast dominated the area and relates easily to groundwater salinity. This effect is of course site specific. Furthermore, as available ground data are mostly present in or around creek ridges and dunes, which are typical freshwater lens features, it should be further noted that there is a bias on techniques that resolve features well under resistive cover.

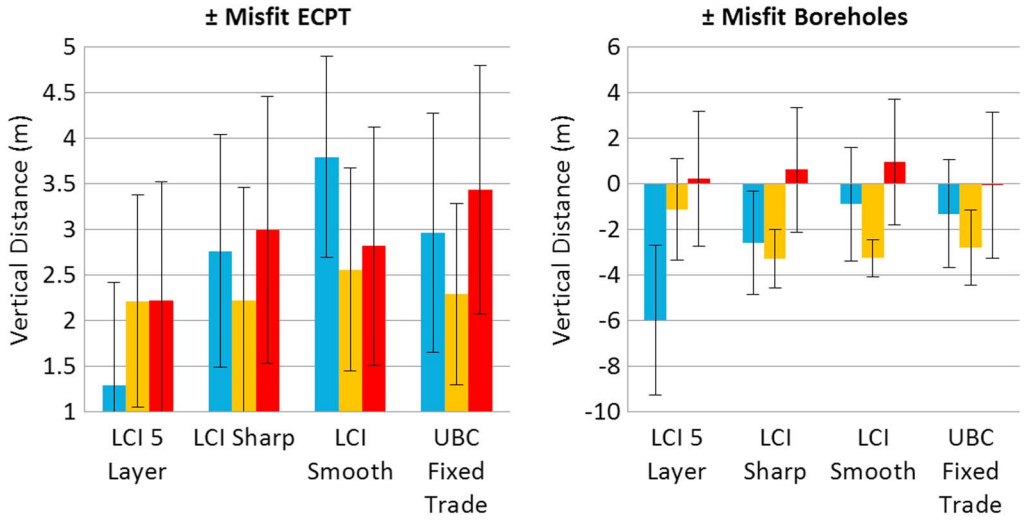

Figure 15. Vertical mismatch (mean ± differences between observed data) of inversion results to extracted interfaces in meters. Red (saline misfit, 1.8 S/m), orange (brackish misfit, 0.54 S/m), and blue (fresh misfit, 0.18 S/m). ECPT = Electric Cone Penetration Test; LCI = laterally constrained inversion; UBC = University of British Columbia.

5.1. Volume Estimates

Fresh-brackish-saline volume estimates primarily illustrate the effect of model smoothness and mapping results. Here it is observed that in the study area, freshwater volume estimates differ by up to 6.5%, or 178 million m^3, between the *sharpest* LCI five-layer and the smoothest LCI smooth results. This effect is primarily caused by the preservation of inversion layers from the 3-D interpolation, resulting in very sharp boundaries (spread over five layers for the few layer inversion) and therefore results in a small brackish zone. As the transition between the fresh-brackish-saline groundwater distributions is naturally smoother (Van Baaren et al., 2018), results suggest that for volume estimates it is preferable to use smooth, multilayer inversions. Furthermore, brackish zone estimates between the LCI sharp and LCI smooth results differed by around 3% or a volume of 82 million m^3. It is therefore shown that by using a multilayer ($\geq$ 20 layers) inversion and carefully selecting the regularization term based on prior knowledge, this smoothing effect can be controlled according to known conditions. This is therefore the recommended approach for volume mapping.

5.2. Accuracy of Salinity Distributions

By plotting inversion results with ECPT and borehole data (Figures 11 and 12), results suggest that LCI smooth and LCI sharp multilayer methods were the most successful at honoring ground data. Predictably, it is shown that sharp interfaces from the few layer inversions, due to having few layers, result in larger misfits. As the ECPT and borehole data are measured every 0.5 and 5 cm, respectively, and the inversions are layered, it is expected that a good match to salinity distribution mapping favors smoother results. Results therefore do not mean that few layer methods are worse—rather for the purposes of mapping smoothly varying groundwater salinities, they were less successful. Results would likely be different if ECPT and borehole data were averaged for each layer of the inversion; however, the smooth distribution of salinity is a common mapping objective—thus, it was decided that a direct comparison was appropriate. Furthermore, given that the province of Zeeland was flooded with saline water relatively recently, and subsequently recharged with fresh groundwater (Berendsen, 2005), the brackish zone is expected to be sharper (or thinner) than many typical hydrological situations—further highlighting the fact that smoother techniques are more suitable in general.

5.3. Interface Mapping

Absolute value results (Figure 14) suggest that interface mapping was remarkably consistent across all inversions, with an average accuracy of around 3 m ($\pm$ 3 m). This could be the result of bias, whereby the regularization term was selected based on the same ECPT data, or additionally it could be an effect of the interpolation method or airborne acquisition system itself. However, given that this consistency is also observed across both ECPT and borehole data, it is unlikely that this error can be attributed to the ground constraints. Overall, the center of the brackish zone interface of 0.54 S/m was resolved better. This is more obvious in the ECPT data, where misfits were observed at between 2.5 and 3 m, compared to the brackish-saline (1.8 S/m) groundwater interface, where these were between 3 and 4.5 m. In terms of resolving the fresh-brackish (0.18 S/m) interface, the ECPT data suggest that few layer and LCI sharp inversions were more successful at a misfit of ~3 m, in contrast to ~4 m from the LCI smooth method. However, borehole data suggest that smoother results from the multilayer inversions worked better. The most likely explanation for this contrasting result may be the fact that the borehole data are located in the dune areas and are deeper. Here the deeper DOI in the dune areas has resulted in thickening of the layers where there are small conductivity contrasts, therefore picking specific interfaces at depth without significant conductivity contrasts becomes more arbitrary for few layer methods. Interestingly, the few layer results are more accurate at resolving the brackish interface in these deeper areas, at ~3 m for the LCI five-layer result. This would suggest that because the few layer inversion changed layer thickness and conductivity in the inversion process, in contrast to the (smoother at depth) 20-layer models, high conductivity contrasts are more likely to be mapped successfully in deeper areas by using few layer methods. As the boreholes are up to 50-m deep, and the multilayer inversion would have a layer thickness of around 10 m at these depths, an error of around ~5 m is expected. It is therefore suggested that unless a strong conductivity contrast is present, trying to map subtle features at greater depth using few layer methods is likely to be less successful. Given that geophysical methods favor strong physical property contrasts, and the dominant contrast in the study area is known to be caused by water salinity (Delsman et al., 2018), this result is therefore expected. In previous hydrogeophysical HEM studies in areas where minimal subsurface information was available, fresh-saline groundwater interfaces were commonly estimated using a conductivity value based on empirical

relationships that relate conductivity to salinity (Siemon, Christiansen, et al., 2009). Our study suggests that selecting the strongest conductivity contrast is preferable over this method and should result in more accurate estimates, albeit with limited flexibility in regard to values (and therefore only a single interface) used. This was undertaken in De Louw et al. (2011) where the sharpest vertical conductivity ratio was used to indicate a *mixing zone* or the brackish groundwater interface as referred to in this study. Furthermore, using the same HEM data, Siemon et al. (2018) found that using this method resulted in a brackish zone mapping error of +0.1 m (± 1.7 m) compared to available ECPT data. Finally, the presence of a strong conductivity contrast is observed in the bimodal distribution of the inversion results, where EC values were grouped mostly between 0–0.3 and $>$ 0.7 S/m.

By using ± values (Figure 15), similar patterns were observed—however, most notably ECPT data suggested that inversion results were consistently too shallow at +2 m (±2 m). In contrast, borehole data showed that all inversions were either around 0 m (±2.5 m) for the saline interface or too deep at −1 to −6 m (± 3 m). This effect results from a number of factors, for example, (1) inherent differences between ground measurement methods, where HEM and direct current methods are more sensitive to horizontal and vertical resistivities, respectively (Siemon, Christiansen, et al., 2009), (2) localized effects on EC measurements such as temperature and lithology, or (3) highly localized features mapped by ground measurements could be *smoothed* by the HEM system or 3-D interpolation—highlighting resolution differences between the methods. Consistent vertical offsets observed in all inversions highlight that while the ground data were a useful quantitative comparison for this study, further research is required to understand this occurrence.

6. Conclusions

Using an extensive amount of available data, the results of this study quantitatively highlight the effects of using different inversion techniques and regularization terms, based on the objectives of a typical hydrogeophysical study. Overall, the four inversion methods tested are generally consistent with one another and are shown to be effective at resolving a number of hydrological features. Differences between multilayer and few layer inversions are observed to be the most prominent, and their suitability depends on specific mapping objectives. To simply map a brackish (0.54 S/m) groundwater interface in shallow or deeper areas with minimal ground data, a few layer inversion type is suggested. Here the area with the sharpest conductivity contrast is likely to be an excellent proxy to this boundary, and no information about FFs is required. If both fresh-brackish (0.18 S/m) and brackish interfaces (0.54 S/m) are required, then a smooth, multilayer inversion is suggested, although it should be noted that due to thick layering at depth, the brackish zone will be less effectively mapped here than with the few layer approach. If the objective is to map a smoothly varying volume of conductivity (therefore salinity distributions), a multilayer inversion type is favored. Further, the choice of regularization terms and the type of multilayer inversion used are shown to affect the estimated brackish zone thickness. If ground data are available, then the smooth inversion regularization term could be chosen accordingly to better match the thickness of the brackish zone. Overall, inversion methods should be selected carefully according to mapping objectives—preferably based on a combination of experience and prior knowledge of the subsurface.

Acknowledgments
This research is financed by the Netherlands Organization for Scientific Research (NWO), which is partly funded by the Ministry of Economic Affairs, and cofinanced by the Netherlands Ministry of Infrastructure and Environment and partners of the Dutch Water Nexus consortium. The airborne data used in this research was acquired for a project called FRESHEM, which was funded by the Province of Zeeland, Deltafonds, Evides, Rijkswaterstaat, municipalities of Zeeland, VNSC, Waterboard Scheldestromen, and ZLTO. A 3-D salinity volume of the FRESHEM project can be downloaded at data.overheid.nl/data/dataset/freshem-zeeland-3d. Gocad software was provided as a grant by Paradigm.

References

Archie, G. E. (1942). The electrical resistivity log as an aid in determining some reservoir characteristics. *Transactions of AIME*, *146*(1), 54–62. https://doi.org/10.2118/942054-G

Auken, E., & Christiansen, A. V. (2004). Layered and laterally constrained 2D inversion of resistivity data. *Geophysics*, *69*(3), 752–761. https://doi.org/10.1190/1.1759461

Auken, E., Christiansen, A. V., Jacobsen, B. H., Foged, N., & Sørensen, K. I. (2005). Piecewise 1D laterally constrained inversion of resistivity data. *Geophysical Prospecting*, *53*(4), 497–506. https://doi.org/10.1111/j.1365-2478.2005.00486.x

Auken, E., Christiansen, A. V., Jacobsen, L. H., & Sørensen, K. I. (2008). A resolution study of buried valleys using laterally constrained inversion of TEM data. *Journal of Applied Geophysics*, *65*(1), 10–20. https://doi.org/10.1016/j.jappgeo.2008.03.003

Ball, L., Smith, B., Minsley, B., Abraham, J., Voss, C., Astley, B., et al. (2010). Airborne electromagnetic and magnetic geophysical survey data of the Yukon Flats and Fort Wainwright Areas, Central Alaska, June 2010, U.S. Geol. Surv. Rep., (June 2010).

Bedrosian, B. P. A., Ball, L. B., Bloss, B. R., & Survey, U. S. G. (2013). Airborne electromagnetic data and processing within Leach Lake basin—Fort Irwin, California.

Bedrosian, P. A., Schamper, C., & Auken, E. (2016). A comparison of helicopter-borne electromagnetic systems for hydrogeologic studies. *Geophysical Prospecting*, *64*(1), 192–215. https://doi.org/10.1111/1365-2478.12262

Begemann, H. K. S. (1965). The friction jacket cone as an aid in determining the soil profile. Proceedings of the 6th International Conference on Soil Mechanics and Foundation Engineering, ICSMFE, Montreal, September 8 - 15 (Vol. 2, pp. 17 - 20).

Berendsen, H. J. A. (2005). The Rhine-Meuse delta at a glance. International Geological Congress Report 2003/2004.

Binley, A., Hubbard, S. S., Huisman, J. A., Revil, A., Robinson, D. A., Singha, K., et al. (2015). The emergence of hydrogeophysics for improved understanding of subsurface processes over multiple scales. *Water Resources Research*, *51*, 3837–3866. https://doi.org/10.1002/2015WR017016

Boesen, T., Auken, E., Christiansen, A. V., Fiandaca, G., Kirkegaard, C., Pfaffhuber, A. A., & Vöge, M. (2018). An efficient 2D inversion scheme for airborne frequency domain data. *Geophysics*, *83*(4), 1–47. https://doi.org/10.1190/geo2017-0280.1

Brodie, R., Green, A., & Munday, T. (2004). *Constrained inversion of resolve electromagnetic data—Riverland, South Australia*. Bentley, WA: CRC LEME.

Brodie, R., & Sambridge, M. (2006). A holistic approach to inversion of frequency-domain airborne EM data. *Geophysics*, *71*(6), G301–G312. https://doi.org/10.1190/1.2356112

Chongo, M., Christiansen, A. V., Tembo, A., Banda, K. E., Nyambe, I. A., Larsen, F., et al. (2015). Airborne and ground-based transient electromagnetic mapping of groundwater salinity in the Machile-Zambezi Basin, southwestern Zambia. *Near Surface Geophysics*, *13*(2089), 383–395. https://doi.org/10.3997/1873-0604.2015024

Constable, S. C. (1987). Occam's inversion: A practical algorithm for generating smooth models from electromagnetic sounding data. *Geophysics*, *52*(3), 289–300. https://doi.org/10.1190/1.1442303

Cox, L. H., Wilson, G. A., & Zhdanov, M. S. (2012). 3D inversion of airborne electromagnetic data. *Geophysics*, *77*(4), WB59–WB69. https://doi.org/10.1190/geo2011-0370.1

De Louw, P. G. B., Eeman, S., Siemon, B., Voortman, B. R., Gunnink, J., van Baaren, E. S., et al. (2011). Shallow rainwater lenses in deltaic areas with saline seepage. *Hydrology and Earth System Sciences*, *15*(12), 3659–3678. https://doi.org/10.5194/hess-15-3659-2011

Delsman, J. R., De Louw, P. G. B., Oude Essink, G. H. P., Stuyfzand, P. J. P. J. J., & Bierkens, M. F. P. (2014). Paleo-modeling of coastal saltwater intrusion during the Holocene: An application to the Netherlands. *Hydrology and Earth System Sciences*, *18*(10), 3891–3905. https://doi.org/10.5194/hess-18-3891-2014

Delsman, J., Van Baaren, E. S., Siemon, B., Dabekaussen, W., Karaoulis, M. C., Pauw, P., et al. (2018). Large-scale, probabilistic salinity mapping using airborne electromagnetics for groundwater management in Zeeland, the Netherlands. *Environmental Research Letters*. https://doi.org/10.1088/1748-9326/aad19e

Faneca Sànchez, M., Gunnink, J. L., van Baaren, E. S., Oude Essink, G. H. P., Siemon, B., Auken, E., et al. (2012). Modelling climate change effects on a Dutch coastal groundwater system using airborne electromagnetic measurements. *Hydrology and Earth System Sciences*, *16*(12), 4499–4516. https://doi.org/10.5194/hess-16-4499-2012

Farquharson, C. G., & Oldenburg, D. W. (2004). A comparison of automatic techniques for estimating the regularization parameter in non-linear inverse problems. *Geophysical Journal International*, *156*(3), 411–425. https://doi.org/10.1111/j.1365-246X.2004.02190.x

Farquharson, C. G., Oldenburg, D. W., & Routh, P. S. (2003). Simultaneous 1D inversion of loop–loop electromagnetic data for magnetic susceptibility and electrical conductivity. *Geophysics*, *68*(6), 1857–1869. https://doi.org/10.1190/1.1635038

Fitterman, D., & Deszcz-Pan, M. (2004). Characterization of saltwater intrusion in South Florida using electromagnetic geophysical methods. 18th Salt Water Intrusion Meet., 405–416. [Available at http://www.swim-site.nl/pdf/swim18/swim18_038.pdf.].

Fitterman, D. V, & Deszcz-Pan, M. (2001). Saltwater intrusion in Everglades National Park, Florida Measured by Airborne Electromagnetic Surveys.

Fraser, D. C. (1978). Resistivity mapping with an airborne multicoil electromagnetic system. *Society of Exploration Geophysicists*, *43*(1), 144–172. https://doi.org/10.1190/1.1440817

Goes, B. J. M., Oude Essink, G. H. P., Vernes, R. W., & Sergi, F. (2009). Estimating the depth of fresh and brackish groundwater in a predominantly saline region using geophysical and hydrological methods, Zeeland, the Netherlands. *Near Surface Geophysics*, *7*(1303), 401–412. https://doi.org/10.3997/1873-0604.2009048

Gunnink, J. L., Bosch, J. H. A., Siemon, B., Roth, B., & Auken, E. (2012). Combining ground-based and airborne EM through artificial neural networks for modelling glacial till under saline groundwater conditions. *Hydrology and Earth System Sciences*, *16*(8), 3061–3074. https://doi.org/10.5194/hess-16-3061-2012

Haber, E., & Oldenburg, D. (2000). A GCV based method for nonlinear ill-posed problems. *Computational Geosciences*, *4*(1), 41–63. https://doi.org/10.1023/A:1011599530422

Haider, K., Engesgaard, P., Sonnenborg, T. O., & Kirkegaard, C. (2014). Numerical modeling of salinity distribution and submarine groundwater discharge to a coastal lagoon in Denmark based on airborne electromagnetic data. *Hydrogeology Journal*, *23*(2), 217–233. https://doi.org/10.1007/s10040-014-1195-0

He, X., Koch, J., Sonnenborg, T. O., Flemming, J., Schamper, C., & Refsgaard, J. C. (2014). Using airborne geophysical data and borehole data. *Water Resources Research*, 1–23. https://doi.org/10.1002/2013WR014593

Herckenrath, D., Fiandaca, G., Auken, E., & Bauer-Gottwein, P. (2013). Sequential and joint hydrogeophysical inversion using a field-scale groundwater model with ERT and TDEM data. *Hydrology and Earth System Sciences*, *17*(10), 4043–4060. https://doi.org/10.5194/hess-17-4043-2013

Hermans, T., Vandenbohede, A., Lebbe, L., Martin, R., Kemna, A., Beaujean, J., et al. (2012). Imaging artificial salt water infiltration using electrical resistivity tomography constrained by geostatistical data. *Journal of Hydrology*, *438-439*, 168–180. https://doi.org/10.1016/j.jhydrol.2012.03.021

Hill, B. (2011). Helicopter electromagnetic and magnetic geophysical survey data, Hunton anticline, south-Central Oklahoma, USGS.

Hodges, G., & Siemon, B. (2008). Comparative analysis of one-dimensional inversions of helicopter-borne frequency-domain electromagnetic data, 5th Int. Conf. Airborne Electromagn.

Huang, H., & Fraser, D. C. (1996). The differential parameter method for multifrequency airborne resistivity mapping. *Geophysics*, *61*(1), 100–109. https://doi.org/10.1190/1.1574674

Jørgensen, F., Scheer, W., Thomsen, S., Sonnenborg, T. O., Hinsby, K., Wiederhold, H., et al. (2012). Transboundary geophysical mapping of geological elements and salinity distribution critical for the assessment of future sea water intrusion in response to sea level rise. *Hydrology and Earth System Sciences*, *16*(7), 1845–1862. https://doi.org/10.5194/hess-16-1845-2012

Li, W. B., Zeng, Z. F., Li, J., Chen, X., Wang, K., & Xia, Z. (2016). 2.5D forward modeling and inversion of frequency-domain airborne electromagnetic data. *Applied Geophysics*, *13*(1), 37–47. https://doi.org/10.1007/s11770-016-0548-y

Macnae, J., King, A., Stolz, N., Osmakoff, A., & Blaha, A. (1998). Fast AEM data processing and inversion. *Exploration Geophysics*, *29*(2), 163–169. https://doi.org/10.1071/EG998163

Marquardt, D. W. (1963). An algorithm for least-squares estimation of nonlinear parameters. *Journal of the Society for Industrial and Applied Mathematics*, *11*(2), 431–441. https://doi.org/10.1137/0111030

McNeil, J. D. (1980). *Electrical conductivity of soils and rocks*, (p. 20). Missisauga, Ont: Geonics Ltd.

Menke, W. (1989). *Geophysical data analysis: Discrete inverse theory*. San Diego: Acad. Press.

Minderhoud, P. S. J., Erkens, G., van Hung, P., Vuong, B. T., Erban, L. E., Kooi, H., et al. (2017). Impacts of 25 years of groundwater extraction on subsidence in the Mekong delta, Vietnam. *Environmental Research Letters*, *12*(6), 13. https://doi.org/10.1088/1748-9326/aa7146

Minsley, B. J. (2011). A trans-dimensional Bayesian Markov chain Monte Carlo algorithm for model assessment using frequency-domain electromagnetic data. *Geophysical Journal International*, *187*(1), 252–272. https://doi.org/10.1111/j.1365-246X.2011.05165.x

Neumann, B., Vafeidis, A. T., Zimmermann, J., & Nicholls, R. J. (2015). Future coastal population growth and exposure to sea-level rise and coastal flooding—A global assessment. *PLoS One*, *10*(3), e0118571. https://doi.org/10.1371/journal.pone.0118571

Oude Essink, G. H. P., Van Baaren, E. S., & De Louw, P. G. B. (2010). Effects of climate change on coastal groundwater systems: A modeling study in the Netherlands. *Water Resources Research*, *46*, W00F04. https://doi.org/10.1029/2009WR008719

Paine, J., & Minty, B. (2005). Airborne hydrogeophysics. *Water*, 333–357. https://doi.org/10.1007/1-4020-3102-5_11

Pauw, P. S., van Baaren, E. S., Visser, M., de Louw, P. G. B., & Essink, G. H. P. O. (2015). Increasing a freshwater lens below a creek ridge using a controlled artificial recharge and drainage system: A case study in the Netherlands. *Hydrogeology Journal*, *23*(7), 1415–1430. https://doi.org/10.1007/s10040-015-1264-z

Pryet, A., Ramm, J., Chilès, J. P., Auken, E., Deffontaines, B., & Violette, S. (2011). 3D resistivity gridding of large AEM datasets: A step toward enhanced geological interpretation. *Journal of Applied Geophysics*, *75*(2), 277–283. https://doi.org/10.1016/j.jappgeo.2011.07.006

Rasmussen, P., Sonnenborg, T. O., Goncear, G., & Hinsby, K. (2013). Assessing impacts of climate change, sea level rise, and drainage canals on saltwater intrusion to coastal aquifer. *Hydrology and Earth System Sciences*, *17*(1), 421–443. https://doi.org/10.5194/hess-17-421-2013

Revil, A., & Glover, P. W. J. (1998). Nature of surface electrical conductivity sandstones, and clays in natural sands. *Geophysical Research Letters*, *25*(5), 691–694. https://doi.org/10.1029/98GL00296

Scheunert, M., Ullmann, A., Afanasjew, M., Börner, R. U., Siemon, B., & Spitzer, K. (2016). A cut-&-paste strategy for the 3-D inversion of helicopter-borne electromagnetic data—I. 3-D inversion using the explicit Jacobian and a tensor-based formulation. *Journal of Applied Geophysics*, *129*, 209–221. https://doi.org/10.1016/j.jappgeo.2016.03.023

Sengpiel, K., & Fluche, B. (1992). Application of airborne electromagnetics to groundwater exploration in Pakistan. *Zeitschrift der Deutschen Geologischen Gesellschaft Band*, *143*, 254–261.

Sengpiel, K., & Siemon, B. (2000). Advanced inversion methods for airborne electromagnetic exploration. *Geophysics*, *65*(6), 1983–1992. https://doi.org/10.1190/1.1444882

Sengpiel, K. P., & Meiser, P. (1981). Locating the freshwater/salt water interface on the island of Spiekeroog by airborne EM resistivity/depth mapping. *Geologisches Jahrbuch*, *C29*, 255–271.

Siemon, B. (2012). Accurate 1D forward and inverse modeling of high-frequency helicopter-borne electromagnetic data. *Geophysics*, *77*(4), WB71–WB87. https://doi.org/10.1190/geo2011-0371.1

Siemon, B., Auken, E., & Christiansen, A. V. (2009). Laterally constrained inversion of helicopter-borne frequency-domain electromagnetic data. *Journal of Applied Geophysics*, *67*(3), 259–268. https://doi.org/10.1016/j.jappgeo.2007.11.003

Siemon, B., Christiansen, A. V., & Auken, E. (2009). A review of helicopter-borne electromagnetic methods for groundwater exploration. *Near Surface Geophysics*, *7*(1303), 629–646. https://doi.org/10.3997/1873-0604.2009043

Siemon, B., Costabel, S., Voß, W., Meyer, U., Deus, N., Elbracht, J., et al. (2015). Airborne and ground geophysical mapping of coastal clays in eastern Friesland, Germany. *Geophysics*, *80*(3), WB21–WB34. https://doi.org/10.1190/geo2014-0102.1

Siemon, B., Steuer, A., Ullmann, A., Vasterling, M., & Voß, W. (2011). Application of frequency-domain helicopter-borne electromagnetics for groundwater exploration in urban areas. *Physics and Chemistry of the Earth*, *36*(16), 1373–1385. https://doi.org/10.1016/j.pce.2011.02.006

Siemon, B., van Baaren, E., Dabekaussen, W., Delsman, J., Karaoulis, M., Gunnink, J., et al. (2018). Automatic identification of fresh-saline groundwater interfaces from airborne EM data in Zeeland (NL). Proc. 78. Jahrestagung der Deutschen Geophysikalischen Gesellschaft, 12.-15.2.2018, Leoben, 53.

Spies, B. R. (1996). Electrical and electromagnetic borehole measurements: A review. *Surveys in Geophysics*, *17*(4), 517–556. https://doi.org/10.1007/BF01901643

Stafleu, J., Maljers, D., Gunnink, J. L., & Busschers, F. S. (2011). 3D modelling of the shallow subsurface of Zeeland, the Netherlands, Netherlands. *Journal of Geosciences*, *16*(1), 5647. https://doi.org/10.5242/iamg.2011.0076

Steuer, A., Siemon, B., & Auken, E. (2009). A comparison of helicopter-borne electromagnetics in frequency- and time-domain at the Cuxhaven valley in Northern Germany. *Journal of Applied Geophysics*, *67*(3), 194–205. https://doi.org/10.1016/j.jappgeo.2007.07.001

Tikhonov, A. N., & Arsenin, V. Y. (1979). Solutions of ill-posed problems. *Society for Industrial and Applied Mathematics*, *21*, 266–267.

Tølbøll, R. J., & Christensen, N. B. (2007). The sensitivity functions of frequency-domain magnetic dipole-dipole systems. *Geophysics*, *72*(2), F45–F56. https://doi.org/10.1190/1.2409623

Van Baaren, E. S., Delsman, J. R., Karaoulis, M., Pauw, P. S., Vermaas, T., Bootsma, H., et al. (2018). *FRESHEM Zeeland - FREsh Salt groundwater distribution by Helicopter ElectroMagnetic survey in the Province of Zeeland*. Deltares report 1209220. Utrecht, Netherlands.

van Weert, F., van der Gun, J., & Reckman, J. (2009). *Global overview of saline groundwater occurrence and genesis*. Utrecht, Paris: IGRAC/UNESCO.

Viezzoli, A., Christiansen, A. V., Auken, E., & Sørensen, K. (2008). Quasi-3D modeling of airborne TEM data by spatially constrained inversion. *Geophysics*, *73*(3), F105–F113.

Vignoli, G., Fiandaca, G., Christiansen, A. V., Kirkegaard, C., & Auken, E. (2015). Sharp spatially constrained inversion with applications to transient electromagnetic data. *Geophysical Prospecting*, *63*(1), 243–255. https://doi.org/10.1111/1365-2478.12185

Vos, P. (2015). Origin of the Dutch coastal landscape: Long-term landscape evolution of the Netherlands during the Holocene, described and visualized in national, regional and local palaeogeographical map series. *GRONINGEN: Barkhuis*. https://doi.org/10.2307/j.ctt2204s8d

Wynn, J. (2005). Mapping ground water in three dimensions—An analysis of airborne geophysical surveys of the upper San Pedro River Basin, Cochise County, Southeastern Arizona.

Yin, C., & Hodges, G. (2007). Simulated Annealing For Airborne EM Data Interpretation. *Fifth Decennial International Conference on Mineral Exploration*, *72*(4), 843–846. https://doi.org/10.1190/1.2736195